

Modified embedded atom method potential for Al, Si, Mg, Cu, and Fe alloys

B. Jelinek, S. Groh,* and M. F. Horstemeyer†

Center for Advanced Vehicular Systems, 200 Research Boulevard, Starkville, Mississippi 39759, USA

J. Houze and S. G. Kim‡

Department of Physics and Astronomy, Mississippi State University, Mississippi State, Mississippi 39762, USA

G. J. Wagner

Sandia National Laboratories, P.O. Box 969, MS 9401, Livermore, California 94551, USA

A. Moitra

Department of Chemical Engineering, The Pennsylvania State University, University Park, Pennsylvania 16802, USA

M. I. Baskes§

Mechanical and Aerospace Engineering, University of California in San Diego, La Jolla, California 92093, USA

(Received 8 March 2012; published 1 June 2012)

A set of modified embedded-atom method (MEAM) potentials for the interactions between Al, Si, Mg, Cu, and Fe was developed from a combination of each element's MEAM potential in order to study metal alloying. Previously published MEAM parameters of single elements have been improved for better agreement to the generalized stacking fault energy (GSFE) curves when compared with *ab initio* generated GSFE curves. The MEAM parameters for element pairs were constructed based on the structural and elastic properties of element pairs in the NaCl reference structure garnered from *ab initio* calculations, with adjustment to reproduce the *ab initio* heat of formation of the most stable binary compounds. The new MEAM potentials were validated by comparing the formation energies of defects, equilibrium volumes, elastic moduli, and heat of formation for several binary compounds with *ab initio* simulations and experiments. Single elements in their ground-state crystal structure were subjected to heating to test the potentials at elevated temperatures. An Al potential was modified to avoid formation of an unphysical solid structure at high temperatures. The thermal expansion coefficient of a compound with the composition of AA 6061 alloy was evaluated and compared with experimental values. MEAM potential tests performed in this work, utilizing the universal atomistic simulation environment (ASE), are distributed to facilitate reproducibility of the results.

DOI: 10.1103/PhysRevB.85.245102

PACS number(s): 61.50.Lt, 62.20.D-, 61.72.J-, 68.35.-p

I. INTRODUCTION

Historically, materials have been developed through the correlation of processing and properties. Several implementations of materials science principles have given birth to an engineering framework for materials design. Over the past two decades, more efficient computational methodologies have been developed and the computational power have increased enormously, making the computational materials design an essential cost-effective tool to design materials properties. Since materials complexities can limit the degree of predictability, several time-scale and length-scale methodologies (hence spatiotemporal hierarchy) for computational materials design naturally evolved (cf. Horstemeyer¹ for a review). Out of several computational methodologies, atomistic simulations not only can predict the materials properties from a statistical viewpoint, but can also quantify the mechanisms of the structure-property relationship. One of the most critical components of atomistic simulations is the interatomic potential, which determines the forces on individual atoms. First-principles calculations certainly are capable of providing very reliable interatomic potentials in a variety of chemical environments. However, realistic simulations of alloy systems, which are essential to reveal many macroscopic materials properties, often require a number of atoms that renders these

methods impractical—they either require too much computer memory or take too long to be completed in a reasonable amount of time. One alternative is to use (semi-)empirical interaction potentials that can be evaluated efficiently, so that the atomistic approaches that use them can, in certain cases, handle systems with more than a million atoms.

The embedded-atom method (EAM) is a widely used atomic level semiempirical model for metals, covalent materials, and impurities.^{2–5} MEAM (Modified EAM) incorporates angular dependency of electron density into EAM. Atomistic simulations of a wide range of elements and alloys have been performed using MEAM potentials. MEAM model was first used for silicon, germanium, and their alloys.⁶ It was applied to 26 single elements⁷ and to silicon-nickel⁸ alloys and interfaces. Gall *et al.*⁹ have used MEAM to model tensile debonding of an aluminum-silicon interface. Lee and Baskes¹⁰ improved MEAM to account for the second nearest-neighbor interactions. Also, Huang *et al.*¹¹ used MEAM and two other potentials to determine defect energetics in β -SiC. MEAM parameters for nickel¹² and molybdenum-silicon system¹³ were determined by Baskes. MEAM potentials for Cu, Ag, Au, Ni, Pd, Pt, Al, and Pb based on the first and the second nearest-neighbor MEAM were constructed by Lee *et al.*¹⁴ Hu *et al.*^{15,16} proposed a new analytic modified EAM many-body

potential and applied it to 17 hcp metals. The structural properties of various polytypes of carbon were described using a MEAM potential by Lee and Lee.¹⁷ Recent work of Lee *et al.*¹⁸ summarized available MEAM potentials for single elements and alloys. Several of these potentials were then used to perform large-scale atomistic simulations to understand the intriguing nature of the ductile and brittle fracture,¹⁹ structure-property relationship,²⁰ dislocation dynamics,^{21,22} and nature of materials fracture.^{23,24}

Aluminum, magnesium, copper, and iron alloys are being used in developing materials with novel properties. The great popularity of these alloys is connected to their general functional properties, mechanical properties, mass density, corrosion resistance, and machinability. Light metal alloys, such as magnesium and aluminum alloys, are now demanded for use in the automotive and aviation industries. They performed remarkably well for the purpose of decreasing the operating expenses and fuel consumption. These alloys usually contain several other minor elements, such as silicon, nickel, and manganese, and are known to have very complex phase compositions. Assessment of such complex systems is a very challenging task, since different constituent elements can form different phases, whose selection depends on the ratio between the constituents and also on a variety of processing and treatment factors.

Contrary to DFT potentials, most of the single element semiempirical potentials do not combine easily into multi-component alloy models. The difficulty of combining single-element EAM potentials into alloy systems comes from the need of their normalization.²⁵ The procedure to form EAM alloy parametrization from single-element potentials was suggested,^{26,27} but it does not guarantee that the resulting potential will be suitable for modeling compounds.²⁸ Alloy potentials usually introduce new parameters for each pair of elements, allowing to fit properties of their binary compounds. The number of parameters to adjust and the number of tests to perform is proportional to the square of the number of constituent elements. In the present MEAM approach, each pair interaction is characterized by a total of 13 parameters (Table V, and the ratio of density scaling factors ρ_0 for constituent elements, Table I). Adoption of the default value $C_{\max} = 2.8$ leads to 9 adjustable parameters for each pair. Comparable angularly dependent potentials for the Fe-Ni system²⁹ also have nine adjustable pair parameters.

While the semiempirical potentials have been developed and tested for binary alloys,^{30–34} binaries, similarly to single-element potentials, may not combine easily into ternaries. Modeling of ternary systems faces a challenge since less experimental properties are available for ternary systems. Ternary potentials are usually examined only at a particular composition range—the number of possible compositions grows to the power of the number of constituent elements. It is also nontrivial to find an equilibrium structure for complex systems of representative size at low temperatures. Ternary potentials are only available for Fe/Ni-Cr-O³⁵ (MEAM), Pu-Ga-He³⁶ (MEAM), Fe-Ti-C/N, Cu-Zr-Ag, Ga-In-N, Fe-Nb-C/N^{37–40} (MEAM), H-C-O⁴¹ (Reactive Force Field, ReaxFF), Ni-Al-H,⁴² Zr-Cu-Al,⁴³ and Fe-Cu-Ni⁴⁴ (EAM) systems. To extend from binaries to ternaries, MEAM provides a ternary screening parameter C^{XYZ} . In the present work, we did not examine ternary systems. Instead, we performed thermal expansion simulations of a compound including all species of the potential. The default values of $C_{\min} = 2.0$ and $C_{\max} = 2.8$ were applied for ternary screening. Since an effort beyond the scope of our project is required for satisfiable validation of the five-element alloy potential under varying temperatures, compositions, and configuration states, we concentrated on basic tests and on providing tools to facilitate reproducibility of the tests.⁴⁵

In the present study, we develop a MEAM potential for aluminum, silicon, magnesium, copper, iron, and their combinations. We fit the potential to the properties of single elements and element pairs, but the model implicitly allows calculations with any combination of elements. We show the applied MEAM methodology in Appendix A. The DFT calculations are described in Sec. II. In Sec. III, the single-element volume-energy curves in basic crystal structures, and also important material properties, such as formation energies of vacancies, self-interstitials, surfaces, and generalized stacking fault energies from MEAM are examined and compared with DFT calculations. In Sec. IV, the MEAM potential parameters for each unlike element pair are initialized to fit the *ab initio* heat of formation, equilibrium volume, and elastic moduli of the hypothetical NaCl reference structure. Heat of formation of binary compounds in a variety of crystal structures from MEAM are thereafter examined and compared with the *ab initio* and experimental results. The MEAM parameters are adjusted to match the DFT formation energy of the most stable

TABLE I. Set of the MEAM potential parameters for single elements. The reference structures for Al, Si, Mg, Cu, and Fe are fcc, diamond, hcp, fcc, and bcc, respectively. E_c is the cohesive energy, a_0 is the equilibrium lattice parameter, A is the scaling factor for the embedding energy, α is the exponential decay factor for the universal energy, $\beta^{(0-3)}$ are the exponential decay factors for the atomic densities, $t^{(0-3)}$ are the weighting factors for the atomic densities, C_{\max} and C_{\min} are screening parameters, ρ_0 is the density scaling factor that is relevant only for element pairs. Definition of these parameters may be found in Ref. 7. Nonzero parameters δ_r in Rose Eqs. (B1)–(B4) were used for Al ($\delta_r = 0.1$) and Fe ($\delta_r = 0.3$), along with $\delta_a = 0.0$.

| elem. | E_c (eV) | a_0 (Å) | A | α | $\beta^{(0)}$ | $\beta^{(1)}$ | $\beta^{(2)}$ | $\beta^{(3)}$ | $t^{(0)}$ | $t^{(1)}$ | $t^{(2)}$ | $t^{(3)}$ | C_{\min} | C_{\max} | ρ_0 |
|-------|------------|-----------|-------|----------|---------------|---------------|---------------|---------------|-----------|-----------|-----------|-----------|------------|------------|----------|
| Al | 3.353 | 4.05 | 1.07 | 4.64 | 2.04 | 3.0 | 6.0 | 1.5 | 1.0 | 4.50 | -2.30 | 8.01 | 0.8 | 2.8 | 1.0 |
| Si | 4.63 | 5.431 | 1.00 | 4.87 | 4.4 | 5.5 | 5.5 | 5.5 | 1.0 | 2.05 | 4.47 | -1.80 | 2.0 | 2.8 | 2.2 |
| Mg | 1.51 | 3.194 | 0.8 | 5.52 | 4.0 | 3.0 | 0.2 | 1.2 | 1.0 | 10.04 | 9.49 | -4.3 | 0.8 | 2.8 | 0.63 |
| Cu | 3.54 | 3.62 | 1.07 | 5.11 | 3.634 | 2.2 | 6.0 | 2.2 | 1.0 | 4.91 | 2.49 | 2.95 | 0.8 | 2.8 | 1.1 |
| Fe | 4.28 | 2.851 | 0.555 | 5.027 | 3.5 | 2.0 | 1.0 | 1.0 | 1.0 | -1.6 | 12.5 | -1.4 | 0.68 | 1.9 | 1.0 |

compounds. The structural and elastic properties for several binary compounds and formation energies of substitutional defects are compared with *ab initio* and experimental results. Finally, we performed thermal expansion simulations of a compound with the composition of an AA 6061 alloy (see Sec. IV C). We conclude with a short summary.

II. AB INITIO CALCULATIONS

Ab initio total energy calculations in this work were based on density functional theory (DFT), using the projector augmented-wave (PAW) method⁴⁶ as implemented in the VASP code.⁴⁷ Exchange-correlation effects were treated by the generalized gradient approximation (GGA) as parameterized by Perdew *et al.*⁴⁸ All DFT calculations were performed in high precision with the plane-wave cut-off energy set to 400 eV in order to achieve the convergence of heat of formation and elastic properties. Integration over the irreducible Brillouin zone was performed using the Γ -centered Monkhorst-Pack scheme⁴⁹ with the size gradually increased to $7 \times 7 \times 7$ for point defects, to $19 \times 19 \times 1$ for surfaces, and to $29 \times 29 \times 29$ to improve convergence of shear moduli at small strains. Elastic constants presented here were obtained without relaxation of atomic positions. Since most of the examined high-energy structures are, at best, metastable, relaxation does not maintain the crystal symmetry, resulting in large energy changes and unphysical elastic constants.

III. MEAM PARAMETERS FOR SINGLE ELEMENTS

The present MEAM parameters for single elements are listed in Table I. The initial values of these parameters were taken from existing MEAM potentials.^{7,14,50,51} The C_{\min} screening parameter for Al, Mg, and Cu was lowered from 2.0 to 0.8 to improve the GSFE curves (see Sec. III E). The Mg potential was adjusted to reproduce the DFT values of hcp, bcc, and fcc energy differences, vacancy formation energy, and $(10\bar{1}0)$ surface formation energy. The Al potential was modified to prevent formation of an unknown structure at elevated temperatures (see Sec. IV C).

A. Energy dependence on volume of single elements in fcc, hcp, bcc, and simple cubic crystal structures

The first test of the validity of MEAM potential for single elements is a comparison of the energy-volume curves in the fcc, hcp, bcc, diamond, and simple cubic crystal structures, shown in Fig. 1. The MEAM potentials appropriately capture the lowest energy structures of Al (fcc), Si (dia), Mg (hcp), Cu (fcc), and Fe (bcc). Also, the equilibrium volumes of several crystal structures from MEAM closely match the DFT results. Better match of DFT energy differences and volume ratios can possibly be obtained by optimization of Si and Cu MEAM parameters. The Fe MEAM potential applied in the present work is a MEAM-p variant of the Fe potential from the recent effort of Lee *et al.*,⁵¹ exhibiting a correct low-temperature phase stability with respect to the pressure. The fcc equilibrium energy and volume from this Fe potential is very close to the bcc equilibrium in order for the structural transition to appear at finite temperature without magnetic contribution. In general,

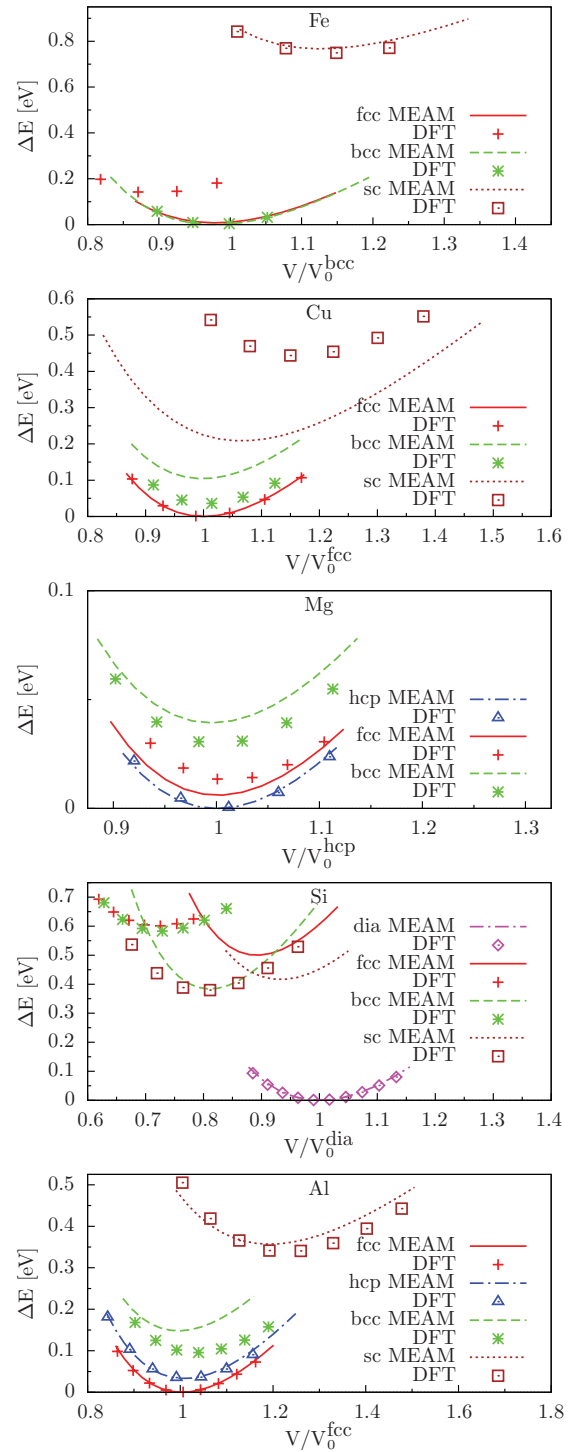


FIG. 1. (Color online) Energy-volume dependence of Al, Si, Mg, Cu, and Fe in fcc, hcp, bcc, diamond, and simple cubic crystal structures relative to the ground state.

the MEAM potentials of the present work reproduced the DFT results for the individual elements fairly well.

B. Vacancies

The formation energy of a single vacancy E_f^{vac} is defined as the energy cost to create a vacancy:

$$E_f^{\text{vac}} = E_{\text{tot}}(N) - N\varepsilon, \quad (1)$$

TABLE II. Calculated single vacancy properties. Single vacancy formation energy E_f^{vac} and formation volume Ω_v values are obtained from the relaxed structures containing single vacancies. Here, Ω_0 is the bulk atomic volume. All energy values are listed in eV. The results from the MEAM calculations are compared with the results from the DFT calculations given inside the parentheses, other simulations, and experiments.

| | E_f^{vac} | | | Ω_v / Ω_0 | |
|----|--------------------|--|-------------------|-----------------------|---------------------------------------|
| | Present | Others | Exp | Present | Others |
| Al | 0.67 (0.5) | 0.68 ^a 0.68 ^b (0.55 ^f) | 0.67 ^g | 0.67 (0.7) | 0.72 ^a 0.61 ^b |
| Si | 3.27 (3.6) | 3.56 ^t 3.67 ^s (3.6 ^c) | 3.6 ⁱ | 0.21 (0.3) | 0.94 ^t |
| Mg | 0.89 (0.7) | 0.59 ^d 0.87 ^b (0.83 ^k) | 0.79 ^e | 0.72 (0.8) | 0.83 ^d 0.87 ^b |
| Cu | 1.10 (1.0) | 1.05 ^q 1.27 ^r (1.03 ^h) | 1.2 ^j | 0.75 (~0.9) | 0.70 ^r 0.74 ^r |
| Fe | 1.65 (2.1) | 1.84 ^l 1.89 ^m (1.95 ⁿ) | 1.53 ^o | 0.47 (~0.8) | 0.6 ^p (0.90 ⁿ) |

^aMEAM results by Ref. 14.

^bCalculated using EAM parameters extracted from Ref. 52.

^cDFT calculation by Ref. 53.

^dAMEAM results by Ref. 15.

^eExperimental results by Ref. 54.

^fDFT results by Ref. 55.

^gExperimental value by Ref. 56.

^hDFT calculation by Ref. 57.

ⁱExperimental value by Ref. 58.

^jExperimental value by Ref. 59.

^kDFT value by Ref. 60.

^lEAM value by Ref. 61.

^mFinnis-Sinclair potential value by Ref. 62.

ⁿDFT value by Ref. 63.

^oExperimental value by Ref. 64.

^pExperimental value referenced in Ref. 62.

^qEAM value by Ref. 65.

^rEAM value by Ref. 66.

^sMEAM value by Ref. 67.

^tMEAM value by Ref. 68.

TABLE III. The formation energies of various Al, Si, Mg, Cu, and Fe self-interstitials. All energy values are given in eV. The results from the MEAM calculations are compared with the DFT results and other classical MD (CMD) simulations.

| Interstitial | DFT | MEAM | CMD | DFT |
|--------------|-----|---------|-------------------|---------|
| Al | | Present | Ref. 52 | Ref. 69 |
| tetrahedral | 3.3 | 3.32 | 3.16 ^a | 2.94 |
| octahedral | 2.8 | 3.26 | 3.06 ^a | 2.82 |
| split (100) | 2.7 | 2.77 | 2.68 ^a | 2.46 |
| Si | | Present | Ref. 72 | Ref. 73 |
| split (110) | 3.7 | 3.71 | 3.88 | 4.7 |
| Mg | | Present | Ref. 52 | Ref. 50 |
| tetrahedral | 2.2 | 1.63 | 1.53 ^a | 1.53 |
| octahedral | 2.2 | 1.57 | 2.16 ^a | 1.29 |
| split (0001) | 2.3 | 1.78 | 1.52 ^a | |
| Cu | | Present | Ref. 65 | Ref. 66 |
| tetrahedral | 3.9 | 3.37 | 2.99 ^a | Ref. 66 |
| octahedral | 3.5 | 2.72 | 2.97 ^a | Ref. 65 |
| split (100) | 3.3 | 2.59 | 2.81 | 3.06 |
| Fe | | Present | Ref. 77 | Ref. 78 |
| tetrahedral | 4.2 | 4.31 | 4.16 ^a | Ref. 78 |
| octahedral | 5.0 | 4.78 | 4.19 ^a | 4.14 |
| split (110) | 3.9 | 3.79 | 3.53 | 4.82 |
| split (111) | 4.9 | 4.28 | 4.02 | 3.64 |
| split (100) | 4.8 | 4.81 | 4.34 | 4.34 |
| | | | | 4.64 |

^aCalculated using parameters from the given reference.

TABLE IV. Surface formation energies for Al, Si, Mg, Cu, and Fe. The units are mJ/m². The second column indicates if the structure was relaxed. Comparisons with other classical MD (CMD), DFT, and experimental values for polycrystalline surfaces and Si facets are also given.

| Surface | Rlx | DFT | MEAM | CMD | DFT | EXP |
|---------|-------|------|---------|----------------------|----------------------|---------|
| Al | | | Present | Ref. 14 | Ref. 52 ^a | Ref. 81 |
| (111) | No | 780 | 820 | | 913 | 1199 |
| (111) | Yes | 780 | 752 | 629 | 912 | 1143 |
| (110) | No | 990 | 1154 | | 1113 | 1271 |
| (110) | Yes | 960 | 1135 | 948 | 1107 | |
| (100) | No | 890 | 1121 | | 1012 | 1347 |
| (100) | Yes | 890 | 1088 | 848 | 1002 | |
| Si | | | Present | Ref. 83 | Ref. 84 | Ref. 85 |
| (111) | No | 1620 | 1254 | 1405 | | 1820 |
| (111) | Yes | 1570 | 1196 | 1405 | | 1740 |
| (100) | No | 2140 | 1850 | 2434 | | 2390 |
| (100) | Yes | 2140 | 1743 | 1489 | | 2390 |
| (100) | 2 × 1 | | 1241 | | 2050 | 1450 |
| Mg | Rlx | | Present | Ref. 15 | Ref. 52 ^a | Ref. 81 |
| (0001) | No | 530 | 780 | | 500 | 792 |
| (0001) | Yes | 530 | 713 | 310 | 499 | 785 |
| (10̄10) | No | 850 | 878 | | 629 | 782 |
| (10̄10) | Yes | 850 | 859 | 316 | 618 | |
| Cu | | | Present | Ref. 87 ^a | Ref. 65 ^a | Ref. 81 |
| (111) | No | 1290 | 1411 | 1185 | 919 | 1952 |
| (111) | Yes | 1290 | 1411 | 1181 | 903 | 1825 |
| (110) | No | 1550 | 1645 | 1427 | 1177 | 2237 |
| (110) | Yes | 1510 | 1614 | 1412 | 1153 | |
| (100) | No | 1440 | 1654 | 1291 | 1097 | 2166 |
| (100) | Yes | 1430 | 1653 | 1288 | 1083 | |
| Fe | | | Present | Ref. 28 ^a | Ref. 77 ^a | Ref. 88 |
| (111) | No | 2760 | 1366 | 1941 | 2012 | 2660 |
| (111) | Yes | 2700 | 1306 | 1863 | 1998 | 2580 |
| (110) | No | 2420 | 1378 | 1434 | 1651 | 2380 |
| (110) | Yes | 2420 | 1372 | 1429 | 1651 | 2370 |
| (100) | No | 2500 | 1233 | 1703 | 1790 | 2480 |
| (100) | Yes | 2480 | 1222 | 1690 | 1785 | 2470 |

^aCalculated using parameters from the given reference.

where $E_{\text{tot}}(N)$ is the total relaxed energy of a system with N atoms containing a vacancy and ε is the energy per atom in the bulk. Cell volume and atomic positions were relaxed in each case. Table II shows the formation energies of a single

vacancy for the fcc Al cell, diamond Si cell, hcp Mg, fcc Cu, and bcc Fe obtained from the MEAM and DFT calculations. The MEAM systems sizes were $5 \times 5 \times 5$ primitive fcc and bcc cells, $3 \times 3 \times 3$ primitive diamond cells, and $8 \times 4 \times 4$

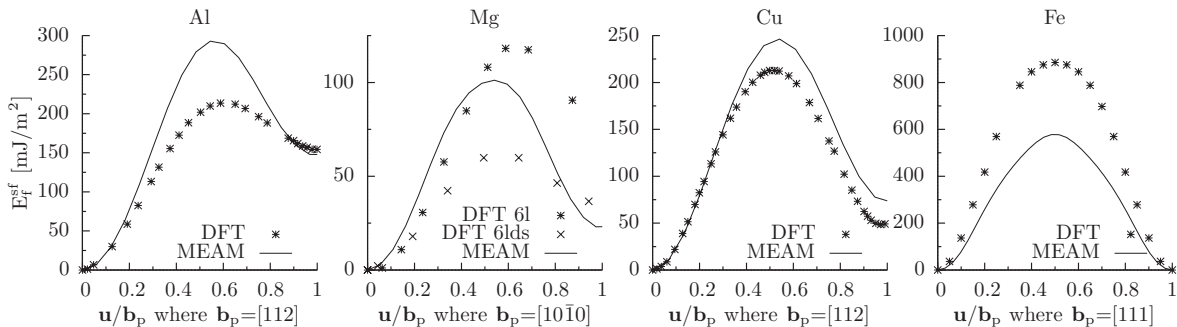


FIG. 2. GSFE curves for Al, Mg, Cu, and Fe obtained with the MEAM potential and compared with the DFT data.

TABLE V. The MEAM potential parameters for element pairs. $\Delta H_{\text{B}1}^{XY}$ is the heat of formation of the NaCl structure (reference) with the type-X and type-Y elements relative to the energies of elemental X and Y in their equilibrium reference state, r_e is their equilibrium nearest neighbor distance, α is the exponential decay factor for the universal energy, C_{\min} and C_{\max} are screening parameters (C^{XYX} denotes type-Y element between two type-X elements). Nonzero parameters $\delta_r = \delta_a = 0.1$ in Rose Eqs. (B1)–(B4) were used for SiFe pair.

| X | Y | $\Delta H_{\text{B}1}^{XY}$ (eV) | r_e^{XY} (Å) | α^{XY} | C_{\min}^{XYX} | C_{\max}^{XYX} | C_{\min}^{YXY} | C_{\max}^{YXY} | C_{\min}^{XXY} | C_{\max}^{XXY} | C_{\min}^{YY} | C_{\max}^{YY} |
|----|----|----------------------------------|----------------|---------------|------------------|------------------|------------------|------------------|------------------|------------------|-----------------|-----------------|
| Al | Si | 0.28 | 2.62 | 4.56 | 0.5 | 2.8 | 2.0 | 2.8 | 2.0 | 2.8 | 2.0 | 2.8 |
| Al | Mg | 0.23 | 2.87 | 4.52 | 2.0 | 2.8 | 0.0 | 2.8 | 2.0 | 2.8 | 0.0 | 2.8 |
| Al | Cu | 0.19 | 2.53 | 4.65 | 0.0 | 2.8 | 2.0 | 2.8 | 2.0 | 2.8 | 2.0 | 2.8 |
| Al | Fe | 0.26 | 2.45 | 4.64 | 0.9 | 2.8 | 0.1 | 2.8 | 2.0 | 2.8 | 2.0 | 2.8 |
| Si | Mg | 0.20 | 2.75 | 4.73 | 1.0 | 2.8 | 1.0 | 2.8 | 2.0 | 2.8 | 2.0 | 2.8 |
| Si | Cu | 0.14 | 2.46 | 4.74 | 0.0 | 2.8 | 0.0 | 2.8 | 2.0 | 2.8 | 2.0 | 2.8 |
| Si | Fe | -0.07 | 2.39 | 5.17 | 1.0 | 2.8 | 1.0 | 2.8 | 2.0 | 2.8 | 0.0 | 2.8 |
| Mg | Cu | 0.23 | 2.63 | 4.70 | 2.0 | 2.8 | 0.0 | 2.8 | 2.0 | 2.8 | 2.0 | 2.8 |
| Mg | Fe | 0.60 | 2.61 | 4.96 | 0.65 | 2.8 | 0.0 | 2.8 | 2.0 | 2.8 | 2.0 | 2.8 |
| Cu | Fe | 0.63 | 2.42 | 5.21 | 2.0 | 2.8 | 0.0 | 2.8 | 2.0 | 2.8 | 2.0 | 2.8 |

orthogonal hcp cells. For the DFT systems, the simulation sizes were $5 \times 5 \times 5$ fcc, $4 \times 4 \times 4$ diamond and bcc, and $4 \times 4 \times 2$ hcp primitive cells.

The vacancy formation energy of Mg was slightly improved in comparison with previous MEAM results.⁵⁰ Overall agreement of vacancy formation energies between MEAM, experiment, and DFT was within a few eV, and the present results are comparable or better than those from other calculations. The reduction in volume due to the formation of a vacancy agrees well with the DFT, except the value for Fe is somewhat low.

C. Self-interstitials

The formation energy of an interstitial point defect E_f^{int} is given by

$$E_f^{\text{int}} = E_{\text{tot}}(N+1) - N\varepsilon_X - \varepsilon_Y, \quad (2)$$

where $E_{\text{tot}}(N+1)$ is the total energy of a system with N type-X bulk atoms plus one impurity atom of type Y inserted at one of the interstitial sites, and ε_X (ε_Y) is the total energy per atom of type X (type-Y) in its most stable bulk structure. The inserted atom Y can be of the same type as the bulk in which case the point defect is called a self-interstitial defect. Self-interstitial formation energies were calculated for Al, Si, Mg, and Cu at the octahedral, tetrahedral, and dumbbell sites. Dumbbell orientations were [100] for fcc, [0001] for hcp, and [110] for bcc and diamond structures. Relaxations of the atomic positions and the volume were also performed, and the DFT and MEAM results are listed in Table III. Similar to the previous calculations, the MEAM systems sizes were $5 \times 5 \times 5$ primitive fcc and bcc cells, $3 \times 3 \times 3$ primitive diamond cells, and $8 \times 4 \times 4$ orthogonal hcp cells. For the DFT systems, the examined sizes were $5 \times 5 \times 5$ fcc primitive cells, $4 \times 4 \times 4$ diamond and bcc primitive cells, and $4 \times 4 \times 2$ hcp primitive cells.

In general, the DFT results are well reproduced or slightly underestimated by the MEAM potentials. According to the present MEAM potential, the most stable form of a self-interstitial defect for fcc Al is a dumbbell along the [100] direction, in agreement with the DFT results and an experimental observation by Jesson *et al.*⁸⁰ The results for Mg are

better than those published previously.^{50,76} The present Mg potential indicates that the tetrahedral site will be most stable in agreement with the DFT calculations. For both Cu and Fe, the new MEAM potential produces the same relative stability of the examined interstitial sites with the DFT calculations.

D. Surfaces

A semi-infinite surface is one of the simplest forms of defects. To test the transferability of the new MEAM potentials, formation energies for several $1 \times 1 \times 7$ surface slabs with 8 Å vacuum layer were computed. Eight atomic layers were used for the Si(111) surface and 12 layers for the

TABLE VI. Structural and elastic properties of element pairs in the reference NaCl (B1) crystal structure from DFT and MEAM calculations. ΔH is the heat of formation in eV/atom, V_0 is the volume per atom in Å³. Elastic constants B_0 , C_{44} , and $(C_{11} - C_{12})/2$ are in GPa.

| pair | method | ΔH | V_0 | B_0 | C_{44} | $\frac{C_{11}-C_{12}}{2}$ |
|------|--------|------------|-------|-------|----------|---------------------------|
| AlSi | DFT | 0.28 | 17.9 | 76.7 | 10 | 76 |
| | MEAM | 0.28 | 18.0 | 76.4 | -13 | 8 |
| AlMg | DFT | 0.42 | 23.7 | 30.9 | -18 | 36 |
| | MEAM | 0.23 | 23.6 | 33.9 | -3 | 35 |
| AlCu | DFT | 0.19 | 16.1 | 77.5 | -18 | 52 |
| | MEAM | 0.19 | 16.2 | 77.4 | -19 | 56 |
| AlFe | DFT | 0.36 | 14.7 | 90.3 | -25 | 105 |
| | MEAM | 0.26 | 14.7 | 92.7 | -27 | 109 |
| SiMg | DFT | 0.41 | 20.9 | 50.6 | -26 | 48 |
| | MEAM | 0.20 | 20.8 | 54.9 | 9 | 61 |
| SiCu | DFT | 0.39 | 14.9 | 99.0 | -29 | 58 |
| | MEAM | 0.14 | 14.9 | 105.9 | 9 | 223 |
| SiFe | DFT | 0.25 | 12.9 | 100.9 | -70 | 112 |
| | MEAM | -0.07 | 13.7 | 157.9 | 65 | 363 |
| MgCu | DFT | 0.23 | 18.5 | 48.7 | -10 | 49 |
| | MEAM | 0.23 | 18.2 | 49.6 | -1 | 61 |
| MgFe | DFT | 0.86 | 17.7 | 50.4 | -23 | 83 |
| | MEAM | 0.60 | 17.8 | 56.5 | -17 | 62 |
| CuFe | DFT | 0.78 | 14.1 | 107.4 | -23 | 134 |
| | MEAM | 0.63 | 14.2 | 111.8 | 10 | 131 |

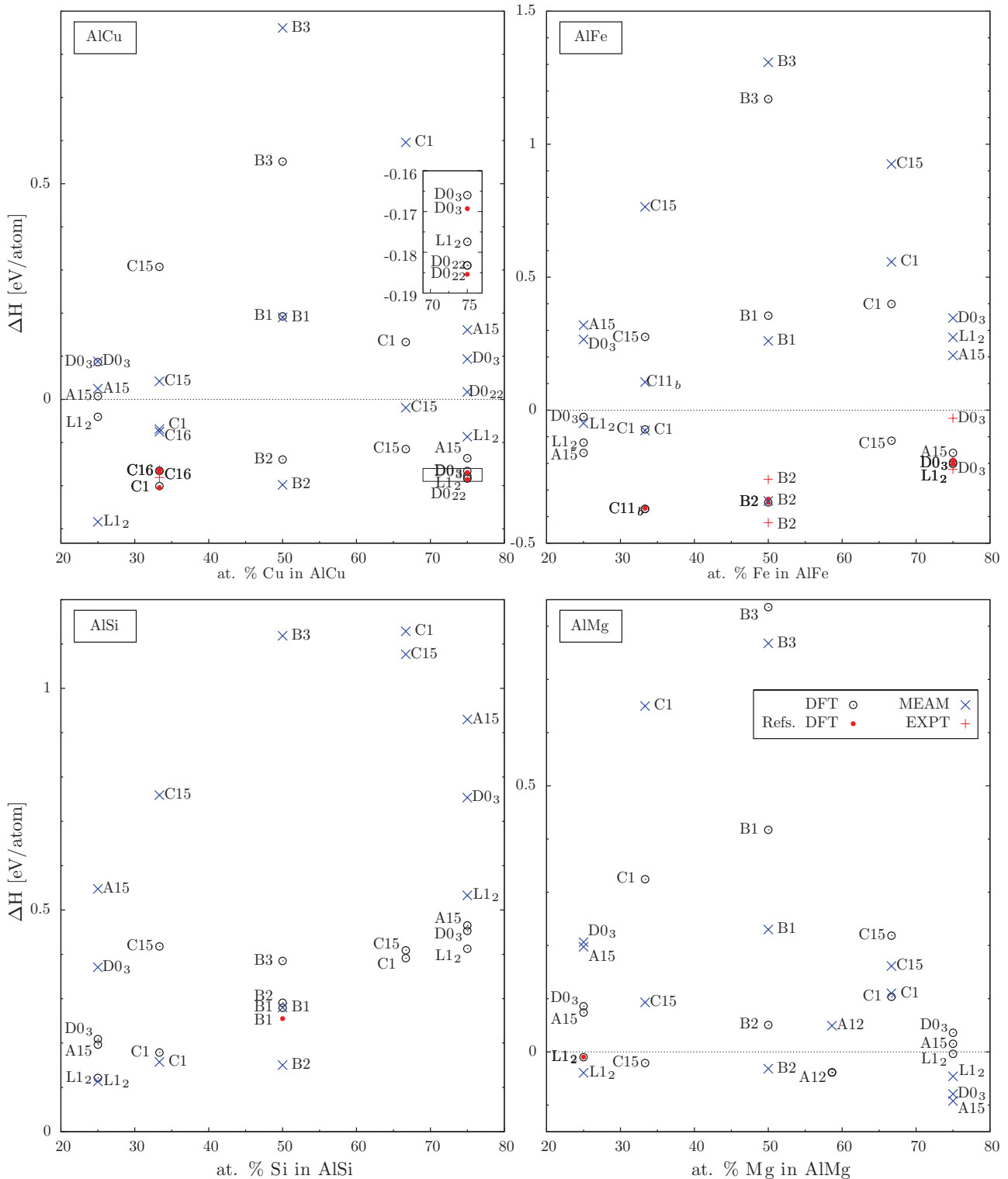


FIG. 3. (Color online) Heat of formation of AlSi, AlMg, AlCu, AlFe binary compounds from MEAM, DFT, and experiments. References: AlSi,⁹ AlMg,¹⁰⁰ AlCu,^{101–104} and AlFe.^{105–107} DFT points are labeled on the left, MEAM and experimental on the right. Values for the most stable compounds are also shown in Table VIII. The inside plot is a magnified portion of a larger plot.

2×1 Si(100) surface reconstruction. The surface formation energy per unit surface area E_{surf} is defined as

$$E_{\text{f}}^{\text{surf}} = \frac{E_{\text{tot}}(N) - N\varepsilon}{A}, \quad (3)$$

where $E_{\text{tot}}(N)$ is the total energy of the structure with two surfaces, N is the number of atoms in the structure, ε is the total energy per atom in the bulk, and A is the total area of both surfaces. Table IV shows the surface formation energies of several surfaces constructed from fcc Al, hcp Mg, fcc Cu,

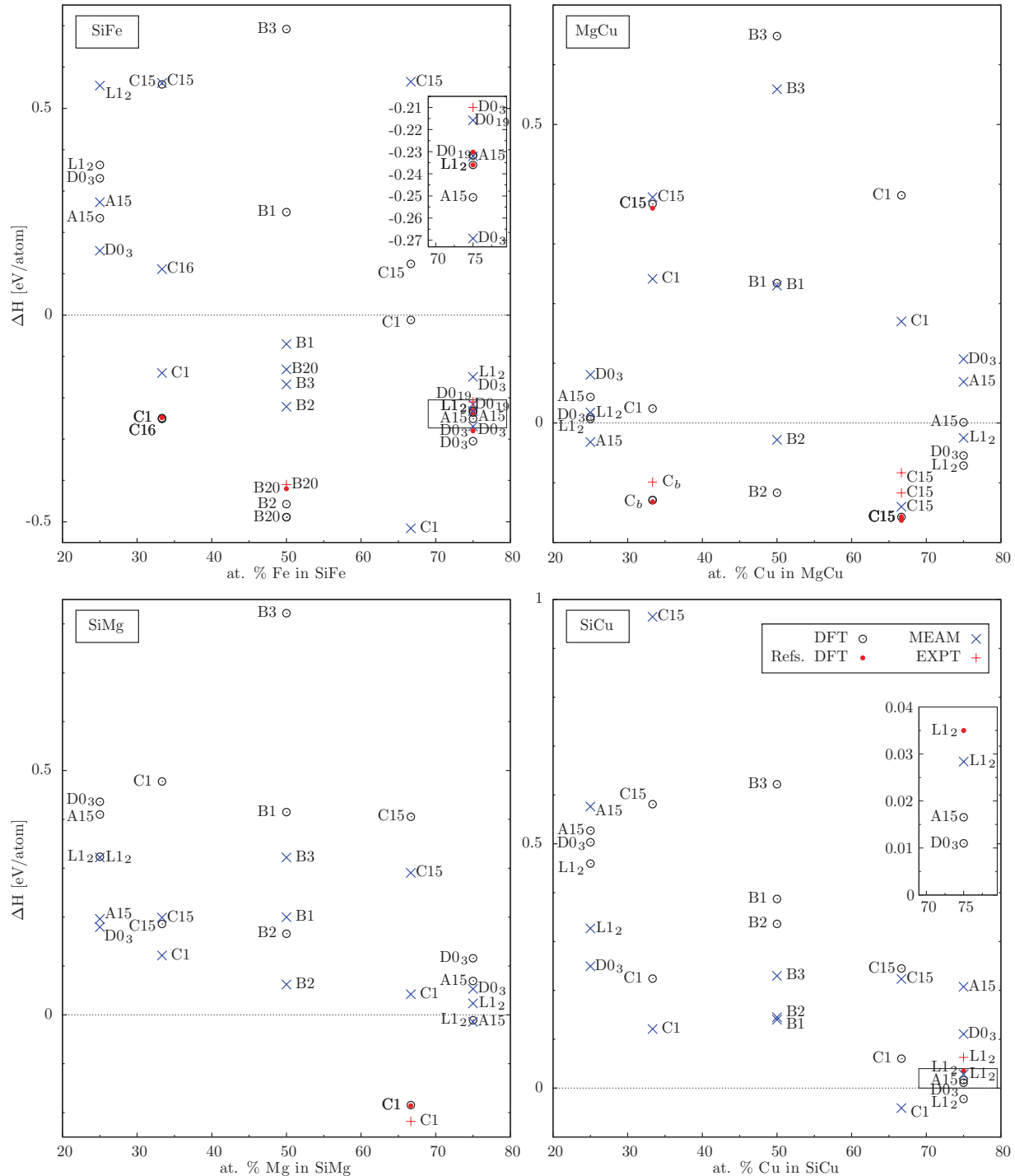


FIG. 4. (Color online) Heat of formation of SiMg, SiCu, SiFe, and MgCu binary compounds from MEAM, DFT, and experiments. References: SiMg,¹⁰⁴ SiCu,^{108,109} SiFe,^{100,110} and MgCu.^{100,111} DFT points are labeled on the left, MEAM and experimental on the right. Values for the most stable compounds are also shown in Table IX. The inside plot is a magnified portion of a larger plot.

and bcc Fe crystals. Results from the present MEAM potentials agree, in the order of magnitude, with the DFT calculations, except for Fe values being underestimated.

The surfaces with lowest energy without reconstruction are identified correctly by the present MEAM potentials. The 2×1 reconstruction of the Si(100) surface leads to symmetric dimers in accord with other Si potentials.⁸⁹ Note that surface formation energies from the present PAW GGA

calculations are lower than our previously published results⁵⁰ using ultrasoft pseudopotentials within local density (LDA) approximation—it is known that GGA leads to surface energies which are 7–16% lower than LDA values for helium and 16–29% lower than the experimental results.^{48,81} A procedure⁹⁰ and new DFT functionals^{91,92} were suggested to correct the errors of LDA and GGA approximations. Similar correction can be applied to vacancy formation

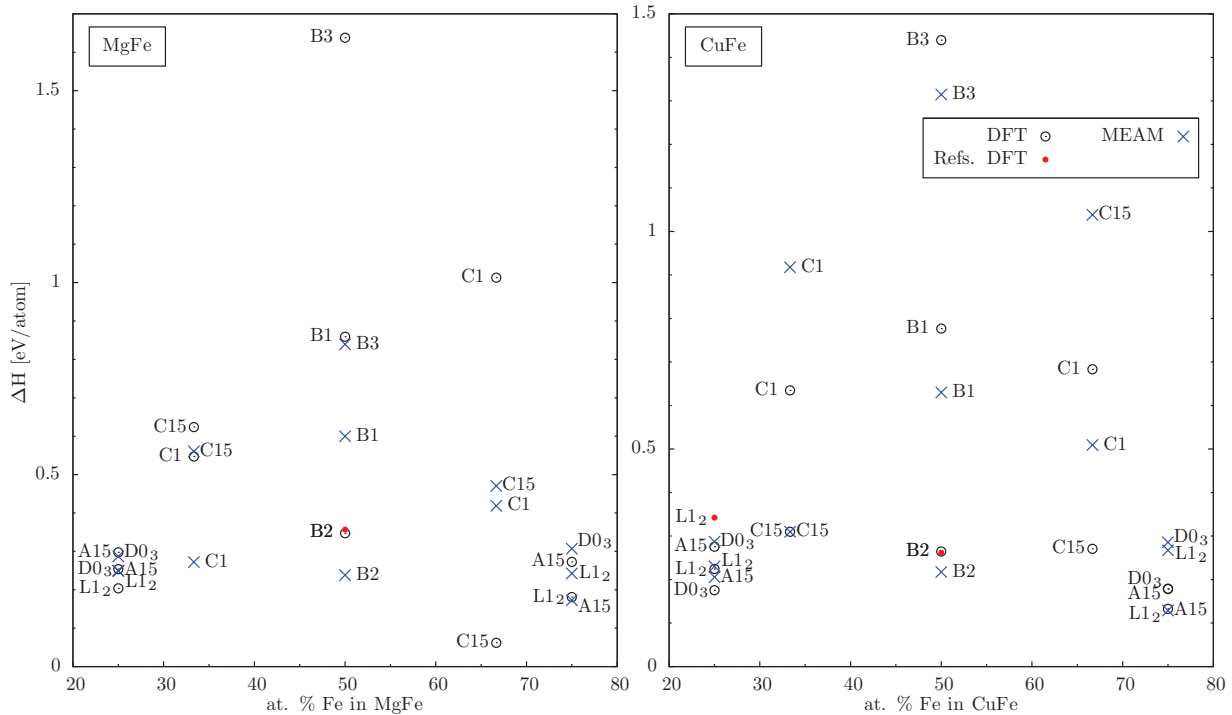


FIG. 5. (Color online) Heat of formation of MgFe and CuFe binary compounds from MEAM and DFT. References: MgFe,¹⁰⁰ CuFe.¹⁰⁰ DFT points are labeled on the left, MEAM on the right. Values for the most stable compounds are also shown in Table IX.

energies,⁹³ but such corrections were not applied in the present study.

E. Stacking faults

Using an assumption of a planar dislocation core, the Peierls-Nabarro model^{94,95} is a powerful theory to quantify the dislocation core properties. In that model, a dislocation is defined by a continuous distribution of shear along the glide plane, and the restoring force acting between atoms on either sides of the interface is balanced by the resultant stress of the distribution. As shown in the recent study of Carrez *et al.*,⁹⁶ a solution of the Peierls-Nabarro model can be obtained numerically by identifying the restoring force to the gradient of the generalized stacking fault energy (GSFE) curve.⁹⁷ In addition, van Swygenhoven *et al.*²⁴ claimed that the nature of slip in nanocrystalline metals cannot be described in terms of an absolute value of the stacking fault energy, and a correct interpretation requires the GSFE curve, which shows the change in energy per unit area of the crystal as a function of

the displacement varied on the slip plane. However, the GSFE curve is not experimentally accessible. Therefore, to model dislocation properties reliably, the GSFE curve calculated with the MEAM potential must reproduce the DFT data.

The stacking fault energy per unit area of a stacking fault E_f^{sf} is defined as

$$E_f^{sf} = \frac{E_{\text{tot}}(N) - N\varepsilon}{A}, \quad (4)$$

where $E_{\text{tot}}(N)$ is the total energy of the structure with a stacking fault, N is the number of atoms in the structure, ε is the total energy per atom in the bulk, and A is the total area of surface.

As a validation test of the MEAM potential, the GSFE curves obtained by molecular statics (MS) were compared with the DFT data by Zimmarman *et al.*⁹⁸ for Al and Cu, by the present authors for Fe, and by Datta *et al.*⁹⁹ for Mg. After lowering the C_{\min} parameter to 0.8, the GSFE curves calculated by MS using the MEAM potential for Al, Cu, and Mg show the skewed sinusoidal shape in agreement with the

TABLE VII. The formation energies of substitutional point defects in Al, Si, Mg, Cu, and Fe. All energy values are given in eV. DFT values are given in parentheses.

| Host | Substitute atom | | | | |
|------|-----------------|-------------|-------------|-------------|-------------|
| | Al | Si | Mg | Cu | Fe |
| Al | | 0.5 (0.5) | -0.2 (0.05) | -1.1 (-0.1) | -1.3 (-0.4) |
| Si | 7.0 (0.9) | | 2.9 (2.4) | 1.9 (2.) | 1.6 (1.9) |
| Mg | -0.7 (0.06) | 0.2 (0.4) | | -0.2 (0.2) | 1.5 (1.1) |
| Cu | 0.7 (-0.7) | 0.8 (-0.2) | 1.1 (-0.2) | | 2.9 (1.4) |
| Fe | 0.2 (-0.7) | -2.9 (-1.1) | 0.8 (1.0) | -0.3 (0.8) | |

TABLE VIII. Structural and elastic properties of element pairs in varying crystal structures from the present DFT and MEAM calculations compared with references and measured values. ΔH is the heat of formation in meV/atom, V_0 is the volume per atom in \AA^3 , and elastic constants B_0 , C_{44} , and $(C_{11} - C_{12})/2$ are in GPa.

| compos. | str. | met. | ΔH | V_0 | B_0 | C_{44} | $\frac{C_{11}-C_{12}}{2}$ |
|--------------------------------|------------------|---|---|--|---------------------------|---------------------|---------------------------|
| Al_3Si | L1 ₂ | DFT | 121 | 16.04 | 74.3 | 24.1 | 9.4 |
| | | MEAM/EAM | 113 | 16.67 | 96.7 | 31.2 | 31.2 |
| Al_2Si | C1 | DFT | 178 | 18.78 | 62.9 | 25.4 | -11.8 |
| | | MEAM/EAM | 157 | 19.17 | 73.6 | 15.3 | 0.0 |
| AlSi | B2 | DFT | 291 | 15.91 | 78.8 | 22.4 | -32.8 |
| | | MEAM/EAM | 150 | 16.25 | 102.1 | 29.1 | -17.0 |
| $\text{Al}_{12}\text{Mg}_{17}$ | A12 | DFT | -39, -35 ¹¹² , -37 ¹¹³ , -48 ¹¹⁴ | 20.12, 18.65 ¹¹² , 20.04 ¹¹³ , 20.25 ¹¹⁴ | 50.1, 49.6 ¹¹⁴ | 20.0 ¹¹⁴ | 28.9 ¹¹⁴ |
| | | MEAM/EAM | 49, -19 ¹¹⁵ , -36 ¹¹⁶ | 21.28, 20.30 ¹¹⁵ | 49.6 ¹¹⁵ | 11.5 ¹¹⁵ | 23.9 ¹¹⁵ |
| | | EXP | -34 ¹¹⁷ | 20.13 ¹¹⁸ , 20.30 ¹¹⁹ | | | |
| | L1 ₂ | DFT | -10, -15 ¹¹² , -9 ³⁰ | 17.80, 16.52 ¹¹² , 17.78 ³⁰ | 63.3 | 35.3 | 31.9 |
| AlMg_3 | | MEAM/EAM | -39, -2 ³⁰ | 19.04, 17.54 ³⁰ | 62.7 | 33.3 | 14.7 |
| | B2 | DFT | -4, -5 ¹¹² , -3 ³⁰ | 20.98, 19.18 ¹¹² , 19.89 ³⁰ | 43.9 | 25.2 | 22.6 |
| AlMg | | MEAM/EAM | -46, 2 ³⁰ | 21.99, 20.98 ³⁰ | 45.0 | 24.9 | 13.8 |
| | | | -32, 90 ¹¹² | 20.29, 19.57 ¹¹² | 50.6 | 32.9 | 8.9 |
| Al_2Cu | C16 | DFT | -166, -170 ¹⁰⁰ , -166 ¹⁰⁴ | 14.95, 14.89 ¹⁰¹ | 96.3 | | |
| | | MEAM/EAM | -163 ¹⁰¹ | | | | |
| | | EXP | -75 | 15.80 | | | |
| | | | -161 ¹²⁰ | 14.90 ¹⁰¹ | | | |
| C1 | DFT | -201, -202 ¹⁰¹ , -204 ¹⁰⁰ | 16.14, 16.12 ¹⁰¹ | 93.1 | 81.6 | 46.0 | |
| | MEAM/EAM | -69 | 17.31 | 77.4 | 43.2 | 7.7 | |
| | EXP | | 15.63 ¹⁰¹ | | | | |
| AlCu_3 | D0 ₂₂ | DFT | -183, -185 ¹⁰⁰ | 12.52 | 123.1 | | |
| | | MEAM/EAM | 17 | 13.08 | | | |
| L1 ₂ | DFT | -177, -219 ¹²¹ | 12.59 | 128.4 | 81.1 | 13.8 | |
| | MEAM/EAM | -87, -229 ¹²¹ | 13.47 | 131.9 | 72.4 | 26.8 | |
| D0 ₃ | DFT | -166, -169 ¹⁰⁰ | 12.60 | 127.9 | 98.4 | 1.1 | |
| | MEAM/EAM | 94 | 12.34 | 107.8 | 88.7 | 4.9 | |
| A15 | DFT | -136 | 12.77 | 124.7 | 34.5 | 102.8 | |
| | MEAM/EAM | 161 | 13.48 | 111.6 | 200.5 | 92.8 | |

TABLE VIII. (*Continued*)

| compos. | str. | met. | ΔH | V_0 | B_0 | C_{44} | $\frac{C_{11}-C_{12}}{2}$ |
|------------------------|------------------|----------|--|--|---|---|---------------------------|
| Al_3Cu | L1 ₂ | DFT | -40 | 15.22 | 89.9 | 23.4 | 61.5 |
| | | MEAM/EAM | -284 | 14.58 | 106.0 | 40.3 | 41.2 |
| AlCu | B2 | DFT | -139 | 13.45 | 108.6 | 31.4 | -15.4 |
| | | MEAM/EAM | -198 | 14.15 | 109.2 | 56.7 | 2.8 |
| AlFe | B2 | DFT | -347, -347 ¹⁰⁰ , -334 ¹²² , -11.86, 11.88 ¹²² , 12.07 ¹²³ , | 174.6, 177.0 ¹²² , 183.0 ¹²⁸ , | 138.8, 165.0 ¹²⁸ , 107.0 ¹⁰⁶ | 61.8, 80.0 ¹²⁸ , 38.1 ¹⁰⁶ | |
| | | | -379 ¹²³ , -420 ¹²⁴ , -400 ¹²⁵ , -338 ¹²⁶ , -311 ¹²⁷ , -1500 ¹⁰⁶ | 11.33 ¹²⁸ , 11.22 ¹²⁴ , 11.65 ¹²⁵ , 11.89 ¹²⁶ , 11.93 ¹²⁷ , 12.19 ¹⁰⁶ | 155.0 ¹²⁷ , 156.0 ¹⁰⁶ | | |
| MEAM/EAM | | | -342, -298 ¹²⁹ , -260 ¹⁰⁵ , -106 ¹³⁰ | 12.88, 12.32 ¹³¹ , 13.92 ¹³⁰ , 11.45 ⁰⁷ | 145.3, 144.0 ¹³¹ , 138.0 ¹³⁰ , 193.0 ⁰⁷ | 111.7, 117.0 ¹³¹ , 110.7 ¹³⁰ | |
| | | | -260 ¹³² , -423 ¹³³ , -250 ¹³⁴ , -280 ¹³⁵ | 12.23 ¹³⁶ | 152.0 ¹³⁷ , 136.0 ¹³⁸ | 127.0 ¹³⁷ , 127.1 ¹³⁸ | |
| AlFe_3 | D0 ₃ | DFT | -202, -203 ¹⁰⁰ , -200 ¹²² , -221 ¹²³ , -230 ¹²⁴ , -202 ¹²⁶ , -201 ¹²⁷ , -1860 ¹⁰⁶ | 11.79, 11.81 ¹²² , 12.01 ¹²³ , 14.65 ¹²⁴ , 11.82 ¹²⁶ , 12.09 ¹²⁷ , 11.57 ¹⁰⁶ | 160.0, 174.0 ¹²² , 151.0 ¹²⁷ , 170.0 ¹⁰⁶ | 140.0, 137.5 ¹⁰⁶ | |
| | | MEAM/EAM | 346, -206 ¹²⁹ , -222 ¹⁰⁵ , -74 ¹³⁰ , -202 ¹³⁴ , -321 ¹³³ | 12.01, 11.77 ¹⁰⁵ , 12.86 ¹³⁰ , 10.80 ⁰⁷ , 12.07 ¹³⁶ | 137.5, 146.0 ¹³⁰ , 229.0 ⁰⁷ , 144.0 ¹³⁸ | 129.0, 162.0 ¹⁰⁵ , 126.3 ¹³⁰ , 131.7 ¹³⁸ | |
| L1_2 | DFT | MEAM/EAM | -196, -187 ¹⁰⁰ , -200 ¹²² , -40 ¹²⁴ , -222 ¹²⁷ , 274, -180 ¹²⁹ | 12.13, 12.14 ¹²² , 14.14 ¹²⁴ , 12.35 ¹²⁷ , 12.88 | 166.3, 158.0 ¹²² , 168.0 ¹²⁷ , 139.5 | 125.1, 96.9 | |
| | | | -161, 205 | 12.08, 12.59 | 156.9, 166.7 | 125.1, 96.9 | |
| AlFe_2 | C15 | DFT | -115, -60 ¹²⁴ | 12.42, 11.43 ¹²⁴ | 130.2, 127.8 | 55.0, 259.2 | |
| | | MEAM/EAM | 925 | 13.67 | 103.5 | 1.8 | |
| Al_3Fe | A15 | DFT | -161, 321 | 13.91, 15.03 | 121.5 | 67.7 | |
| | | MEAM/EAM | -49 | 14.83 | 108.5 | 59.4 | |
| L1_2 | DFT | MEAM/EAM | -122, -150 ¹²⁴ , -105 ¹²⁷ | 13.68, 13.07 ¹²⁴ , 13.69 ¹²⁷ | 126.5, 98.8 ¹²⁷ | 85.9 | |
| | | | 266 | 14.81 | 93.8 | 57.7 | |
| D0_3 | DFT | MEAM/EAM | -25, -99 ¹²³ , -13 ¹²⁷ | 13.38, 13.57 ¹²³ , 13.35 ¹²⁷ | 126.0, 119.6 ¹²⁷ | 91.4 | |
| | | | -371, -420 ¹²⁴ | 12.78, 12.35 ¹²⁴ , 12.80 ¹³⁹ | 149.0 | -48.3 | |
| Al_2Fe | C11 _b | DFT | MEAM/EAM | 106 | 14.71 | 57.7 | -31.1 |
| | | | -72 | 15.25, 16.12 | 90.4 | 47.5 | |
| C1 | DFT | MEAM/EAM | -76 | | | | |
| | | | | | | | |

TABLE IX. Structural and elastic properties of element pairs in varying crystal structures from the present DFT and MEAM calculations compared with references and measured values. ΔH is the heat of formation in meV/atom, V_0 is the volume per atom in \AA^3 , and elastic constants B_0 , C_{44} , and $(C_{11} - C_{12})/2$ are in GPa.

| compos. | str. | met. | ΔH | V_0 | B_0 | C_{44} | $\frac{C_{11}-C_{12}}{2}$ |
|--------------------|------------------|----------|---|-------|-------|----------|---------------------------|
| SiMg ₂ | C1 | DFT | -185, -186 ¹⁰⁴ | 21.41 | 54.1 | 47.6 | 47.3 |
| | | MEAM/EAM | 42 | 23.05 | 47.8 | 20.9 | 32.2 |
| | | EXP | -225 ¹²⁰ | | | | |
| SiMg ₃ | L1 ₂ | DFT | -11 | 19.29 | 50.8 | 29.9 | 37.1 |
| | | MEAM/EAM | 24 | 20.70 | 57.5 | 23.5 | 21.8 |
| | A15 | DFT | 69 | 20.09 | 44.1 | 9.3 | 31.8 |
| | | MEAM/EAM | -14 | 21.25 | 56.3 | 32.2 | 33.9 |
| SiCu ₃ | L1 ₂ | DFT | -22, 35 ¹⁰⁹ | 12.18 | 137.3 | 65.0 | 38.1 |
| | | MEAM/EAM | 28 | 13.37 | 134.9 | 64.4 | 33.0 |
| | | EXP | 63 ¹⁰⁸ | | | | |
| SiCu ₂ | C1 | DFT | 60 | 14.26 | 111.9 | 76.3 | 23.1 |
| | | MEAM/EAM | -41 | 14.81 | 102.8 | 97.9 | 16.2 |
| SiFe | B20 | DFT | -489, -484 ¹⁰⁰ , -420 ¹¹⁰ | 11.04 | 226.5 | | |
| | | MEAM/EAM | -132 | 13.11 | | | |
| | | EXP | -410 ¹¹⁰ | | | | |
| | B2 | DFT | -457 | 10.55 | 231.9 | 87.0 | 155.8 |
| | | MEAM/EAM | -222 | 13.09 | 177.7 | 36.2 | 225.3 |
| SiFe ₃ | D0 ₃ | DFT | -305, -315 ¹⁰⁰ , -280 ¹¹⁰ | 10.99 | 204.5 | 142.4 | 54.5 |
| | | MEAM/EAM | -269 | 12.03 | 169.2 | 91.6 | 36.6 |
| | | EXP | -210 ¹¹⁰ | | | | |
| | A15 | DFT | -251 | 11.44 | 173.3 | 72.3 | 125.3 |
| | | MEAM/EAM | -232 | 12.28 | 190.1 | 47.6 | 119.9 |
| | L1 ₂ | DFT | -236, -236 ¹⁰⁰ | 11.38 | 188.4 | 116.0 | 26.6 |
| | | MEAM/EAM | -149 | 11.80 | 188.6 | 65.1 | 135.8 |
| | D0 ₁₉ | DFT | -232, -230 ¹⁰⁰ | 11.28 | 160.1 | | |
| | | MEAM/EAM | -216 | 12.05 | | | |
| Si ₂ Fe | C1 | DFT | -249, -248 ¹⁰⁰ | 13.05 | 169.4 | 136.8 | 15.5 |
| | | MEAM/EAM | -140 | 15.53 | 158.7 | 95.7 | 41.3 |
| | C16 | DFT | -251, -248 ¹⁰⁰ | 12.39 | 170.6 | | |
| | | MEAM/EAM | 111 | 13.64 | | | |
| SiFe ₂ | C1 | DFT | -12 | 12.95 | 159.6 | 82.6 | -1.4 |
| | | MEAM/EAM | -516 | 12.95 | 182.4 | 154.6 | 226.8 |
| Mg ₂ Cu | C _b | DFT | -129, -131 ¹⁰⁰ , -132 ¹⁴⁰ , -137 ¹¹¹ | 18.13 | 57.1 | | |
| | | EXP | -99 ¹⁴¹ | | | | |
| MgCu ₂ | C15 | DFT | -157, -160 ¹⁰⁰ , -163 ¹¹¹ , -157 ¹⁴⁰ | 14.58 | 90.6 | 45.4 | 25.2 |
| | | MEAM/EAM | -140 | 14.50 | 104.7 | 21.5 | -12.0 |
| | | EXP | -117 ¹⁴¹ , -83 ¹⁴² | | | | |
| MgCu | B2 | DFT | -117 | 15.65 | 69.3 | 60.3 | 16.9 |
| | | MEAM/EAM | -28 | 15.56 | 73.6 | 51.1 | -11.6 |
| MgCu ₃ | L1 ₂ | DFT | -71 | 13.49 | 96.6 | 62.6 | 21.5 |
| | | MEAM/EAM | -25 | 13.81 | 103.9 | 42.5 | 29.0 |
| | D0 ₃ | DFT | -54 | 13.52 | 96.5 | 75.2 | 0.3 |
| | | MEAM/EAM | 107 | 13.43 | 95.7 | 64.1 | -22.4 |

TABLE IX. (*Continued*)

| compos. | str. | met. | ΔH | V_0 | B_0 | C_{44} | $\frac{C_{11}-C_{12}}{2}$ |
|--------------------|-----------------|----------|-------------------------|-------|-------|----------|---------------------------|
| MgFe ₂ | C15 | DFT | 62 | 13.58 | 91.4 | 72.0 | 53.4 |
| | | MEAM/EAM | 471 | 14.79 | 95.8 | 322.9 | 605.7 |
| MgFe ₃ | L1 ₂ | DFT | 181 | 13.11 | 122.6 | 96.9 | 14.0 |
| | | MEAM/EAM | 243 | 13.65 | 116.4 | 64.5 | 45.5 |
| Mg ₃ Fe | L1 ₂ | DFT | 204 | 18.29 | 51.6 | 52.1 | 18.9 |
| | | MEAM/EAM | 249 | 19.08 | 54.5 | 30.0 | 23.1 |
| MgFe | B2 | DFT | 347, 357 ¹⁰⁰ | 15.39 | 71.4 | 68.7 | -25.4 |
| | | MEAM/EAM | 238 | 15.82 | 86.4 | 63.2 | 13.7 |
| CuFe ₃ | L1 ₂ | DFT | 133 | 11.73 | 132.5 | 99.9 | 6.8 |
| | | MEAM/EAM | 267 | 11.78 | 172.6 | 80.5 | 68.0 |
| | A15 | DFT | 178 | 11.95 | 137.6 | 54.2 | 134.7 |
| | | MEAM/EAM | 129 | 12.26 | 192.3 | 70.5 | 155.2 |
| Cu ₃ Fe | D0 ₃ | DFT | 175 | 12.10 | 139.2 | 105.5 | -2.0 |
| | | MEAM/EAM | 287 | 11.59 | 134.0 | 130.8 | 20.7 |
| | L1 ₂ | DFT | 224, 342 ¹⁰⁰ | 12.16 | 135.2 | 60.7 | -0.0 |
| | | MEAM/EAM | 230 | 12.01 | 153.2 | 66.7 | 71.7 |
| CuFe | B2 | DFT | 264, 262 ¹⁰⁰ | 11.88 | 211.4 | 108.7 | -52.0 |
| | | MEAM/EAM | 217 | 12.10 | 161.7 | 105.6 | 45.7 |

DFT predictions (see Fig. 2) illustrating reasonable agreement with the DFT GSFE curves.

IV. MEAM PARAMETERS FOR ELEMENT PAIRS

The MEAM potential parameters for each element pair were initialized to match the *ab initio* heat of formation, equilibrium volume, bulk modulus, and elastic moduli in the hypothetical NaCl reference structure, which was chosen for its simplicity. Since the equilibrium volume, cohesive energy, and bulk modulus of the NaCl structure are directly related to MEAM parameters, they can be reproduced exactly. An improved agreement of the shear moduli from MEAM and *ab initio* simulations was achieved in some cases by adjusting the electron density scaling factor ρ_0 . Then, heat of formation of binary compounds in a variety of crystal structures from MEAM were examined and compared with the *ab initio* results. To correlate the MEAM results with the lowest formation energies of the compounds from DFT calculations, the MEAM screening and $\Delta H_{\text{BI}}^{XY}$ parameters for element pairs were adjusted. The final MEAM parameters are given in Table V. The predicted MEAM properties for the NaCl reference structure are compared with DFT results in Table VI, and show that, in general, the MEAM heat of formation, bulk modulus, and equilibrium volume reproduce the DFT results well. In contrast, the shear elastic constants are not well reproduced. In fact, the sign of the shear elastic constant, representing crystal stability, is frequently in disagreement with the DFT results. This is really not a significant problem as the NaCl structure

does not exist in nature. A more important criteria for success of these potentials is how they perform for lower energy crystal structures. We address this issue in the next section.

A. Heat of formation for binary compounds

The alloy phases that the MEAM potential predicts as most likely to form at the temperature $T = 0$ K are those with the lowest heat of formation per atom, ΔH , which is defined as

$$\Delta H = \frac{E_{\text{tot}}(N_X + N_Y) - N_X \varepsilon_X - N_Y \varepsilon_Y}{N_X + N_Y}, \quad (5)$$

E_{tot} is the total energy of the simulation cell, N_X and N_Y are the numbers of type-X and type-Y atoms in the cell, ε_X and ε_Y are the total energies per atom for type X and type Y in their ground-state bulk structures, respectively.

To check the validity of our new potentials, we computed the heat of formation per atom for many intermetallic phases of all alloy pairs. The total energy values in Eq. (5) for B1, B2, B3, C1, C15, D0₃, A15, L1₂, and other relevant structures were evaluated at the optimal atomic volume for each structure. Heat of formation for basic binary compounds based on the new MEAM potential and DFT results were calculated and compared with experimental values (see Figs. 3–5). The DFT and MEAM results for the phases with lowest ΔH are also shown in Tables VIII and IX.

The agreement between MEAM and DFT is quite satisfactory. In most cases, the MEAM results preserve the order of stability predicted by the DFT results. The differences in the heat of formation per atom from the MEAM and DFT

results are less than 0.5 eV at most. In general, the atomic volumes predicted by MEAM agree at least qualitatively with the DFT and experimental results. The MEAM calculations of the bulk moduli also agree semiquantitatively with DFT and experimental results, usually within 20%. Predicted shear moduli usually follow the DFT and experimental results, but in some cases, there is significant disagreement.

B. Substitutions

The formation energy of a substitutional point defect E_f^{sub} , in the case of the substitution of a type-X atom of the host with a type-Y atom, is defined by

$$E_f^{\text{sub}} = E_{\text{tot}}[(N - 1) + 1] - (N - 1)\varepsilon_X - \varepsilon_Y, \quad (6)$$

where $E_{\text{tot}}[(N - 1) + 1]$ is the total energy of a system of $N - 1$ host type-X atoms and one type-Y atom that replaced type-X atom in the original bulk position, ε_X and ε_Y are the total energies per atom for type-X and type-Y atoms in their ground-state bulk structures. Table VII shows the results of substitutional defect calculations using the MEAM potentials and the DFT results. In general, the MEAM results qualitatively agree with the DFT results. In a number of cases of small heat of formation, MEAM indicates a small heat but of the incorrect sign. The most significant error is for Al in Si where MEAM predicts a large endothermic heat and DFT predicts a much smaller value, otherwise there is general agreement.

C. Finite temperature tests

Real-life applications of MD potentials require extensive testing at finite temperatures. Basic finite-temperature tests of the potentials, in accord with recommendations of Lee *et al.*,¹⁸ revealed formation of an unknown solid structure when the temperature of fcc Al crystal was increased to 800 K under zero pressure conditions. To prevent formation of this structure, $\beta^{(1)}$ and $t^{(1)}$ parameters of Al were adjusted. Heating of other elements under zero-pressure conditions did not result in forming new structures.

To test a system including all components of the new potential, an 20–100 °C average thermal expansion coefficient of a model system with the composition similar to AA 6061 alloy (see Table X) was evaluated and compared with experimental data. Atoms of constituents were placed in the substitutional positions of a $20 \times 20 \times 20$ fcc Al cell.

TABLE X. Composition limits of AA 6061 alloy (see Ref. 143) and a model system used to estimate thermal expansion coefficient.

| Element | Limits | | |
|---------|-------------|--------------|---------------|
| | low (wt. %) | high (wt. %) | Model (wt. %) |
| Si | 0.40 | 0.8 | 0.51 |
| Mg | 0.8 | 1.2 | 1.00 |
| Cu | 0.15 | 0.40 | 0.30 |
| Fe | no | 0.7 | 0.50 |
| Mn | no | 0.15 | 0.00 |
| Cr | 0.04 | 0.35 | 0.00 |
| Zn | no | 0.25 | 0.00 |
| Ti | no | 0.15 | 0.00 |

TABLE XI. Thermal expansion coefficient of single crystal Al and AA 6061 alloy between 20 °C and 100 °C in the units of $\mu\text{m}/\text{m}/\text{K}$.

| | CMD | | Exp | |
|---------|---------|----------|----------|----------|
| | present | Ref. 144 | Ref. 145 | Ref. 143 |
| Al fcc | 14.4 | 15–25 | 25.4 | 23.6 |
| AA 6061 | 14.6 | | | 23.6 |

The system was heated from –200 °C to 20 °C (and 100 °C) over the interval of 0.1 ns, and then equilibrated at 20 °C (and 100 °C) for 1 ns under zero pressure conditions. Table XI shows the values of 20–100 °C average thermal expansion coefficients. The MEAM result for single crystal Al is in the lower range of other MD potentials and experiments. Since Al is a dominant element of the AA 6061 alloy, the thermal expansion coefficient for alloy is similarly underestimated, possibly also due to imperfections of the structure of the real material.

V. CONCLUSIONS

In this study, we developed MEAM potentials for the pair combinations of aluminum, silicon, magnesium, copper, and iron. The MEAM formalism allows any of these potentials to be combined to enable prediction of multicomponent alloy properties. These potentials reproduce a large body of elemental and binary properties from DFT calculations at the temperature of 0 K and experimental results. Basic finite-temperature tests of the single element potentials and their alloy combinations were also performed. With focus to facilitate reproducibility of the presented results,⁴⁵ and subject to further testing and improvements, these potentials are one step toward designing multicomponent alloys by simulations.

ACKNOWLEDGMENT

The authors are grateful to the Center for Advanced Vehicular Systems at Mississippi State University for supporting this study. Computer time allocation has been provided by the High Performance Computing Collaboratory (HPC²) at Mississippi State University. Computational package LAMMPS¹⁴⁶ with ASE¹⁴⁷ interface was used to perform MD simulations. Much appreciated tests of the new MEAM potentials, including the high-temperature simulations of Al that revealed formation of unknown Al phase at 800 K, were performed by Chandler Becker and Tanner Hamann at the Metallurgy Division of the Material Measurement Laboratory, National Institute of Standards and Technology (NIST). Comparison of *ab initio* elastic constants and related discussion with Hannes Schweiger from Materials Design are also appreciated. Classical MD potentials from other authors examined in this study were downloaded from the Interatomic Potentials Repository Project database.¹⁴⁸ Sandia National Laboratories is a multiprogram laboratory managed and operated by Sandia Corporation, a wholly owned subsidiary of Lockheed Martin Corporation, for the US Department of Energy's National

Nuclear Security Administration under contract DE-AC04-94AL85000.

APPENDIX A: MEAM THEORY

The total energy E of a system of atoms in the MEAM⁷ is approximated as the sum of the atomic energies

$$E = \sum_i E_i. \quad (\text{A1})$$

The energy of atom i consists of the embedding energy and the pair potential terms:

$$E_i = F_i(\bar{\rho}_i) + \frac{1}{2} \sum_{j \neq i} \phi_{ij}(r_{ij}). \quad (\text{A2})$$

F is the embedding function, $\bar{\rho}_i$ is the background electron density at the site of atom i , and $\phi_{ij}(r_{ij})$ is the pair potential between atoms i and j separated by a distance r_{ij} . The embedding energy $F_i(\bar{\rho}_i)$ represents the energy cost to insert atom i at a site where the background electron density is $\bar{\rho}_i$. The embedding energy is given in the form

$$F_i(\bar{\rho}_i) = \begin{cases} A_i E_i^0 \bar{\rho}_i \ln(\bar{\rho}_i) & \text{if } \bar{\rho}_i \geq 0, \\ -A_i E_i^0 \bar{\rho}_i & \text{if } \bar{\rho}_i < 0, \end{cases} \quad (\text{A3})$$

where the sublimation energy E_i^0 and parameter A_i depend on the element type of atom i . The background electron density $\bar{\rho}_i$ is given by

$$\bar{\rho}_i = \frac{\rho_i^{(0)}}{\rho_i^0} G(\Gamma_i), \quad (\text{A4})$$

where

$$\Gamma_i = \sum_{k=1}^3 t_i^{(k)} \left(\frac{\rho_i^{(k)}}{\rho_i^{(0)}} \right)^2 \quad (\text{A5})$$

and

$$G(\Gamma) = \begin{cases} \sqrt{1 + \Gamma} & \text{if } \Gamma \geq -1, \\ -\sqrt{|1 + \Gamma|} & \text{if } \Gamma < -1. \end{cases} \quad (\text{A6})$$

The zeroth and higher-order densities, $\rho_i^{(0)}$, $\rho_i^{(1)}$, $\rho_i^{(2)}$, and $\rho_i^{(3)}$ are given in Eq. (A9). The composition-dependent electron density scaling ρ_i^0 is given by

$$\rho_i^0 = \rho_{i0} Z_{i0} G(\Gamma_i^{\text{ref}}), \quad (\text{A7})$$

where ρ_{i0} is an element-dependent density scaling, Z_{i0} is the first nearest-neighbor coordination of the reference system, and Γ_i^{ref} is given by

$$\Gamma_i^{\text{ref}} = \frac{1}{Z_{i0}^2} \sum_{k=1}^3 t_i^{(k)} s_i^{(k)}, \quad (\text{A8})$$

where $s_i^{(k)}$ is the shape factor that depends on the reference structure for atom i . Shape factors for various structures are specified in the work of Baskes.⁷ The partial electron densities are given by

$$\rho_i^{(0)} = \sum_{j \neq i} \rho_j^{a(0)}(r_{ij}) S_{ij}, \quad (\text{A9a})$$

$$(\rho_i^{(1)})^2 = \sum_{\alpha} \left[\sum_{j \neq i} \rho_j^{a(1)} \frac{r_{ij\alpha}}{r_{ij}} S_{ij} \right]^2, \quad (\text{A9b})$$

$$(\rho_i^{(2)})^2 = \sum_{\alpha, \beta} \left[\sum_{j \neq i} \rho_j^{a(2)} \frac{r_{ij\alpha} r_{ij\beta}}{r_{ij}^2} S_{ij} \right]^2 - \frac{1}{3} \left[\sum_{j \neq i} \rho_j^{a(2)}(r_{ij}) S_{ij} \right]^2, \quad (\text{A9c})$$

$$(\rho_i^{(3)})^2 = \sum_{\alpha, \beta, \gamma} \left[\sum_{j \neq i} \rho_j^{a(3)} \frac{r_{ij\alpha} r_{ij\beta} r_{ij\gamma}}{r_{ij}^3} S_{ij} \right]^2 - \frac{3}{5} \sum_{\alpha} \left[\sum_{j \neq i} \rho_j^{a(3)} \frac{r_{ij\alpha}}{r_{ij}} S_{ij} \right]^2, \quad (\text{A9d})$$

where $r_{ij\alpha}$ is the α component of the displacement vector from atom i to atom j . S_{ij} is the screening function between atoms i and j and is defined in Eq. (A16). The atomic electron densities are computed as

$$\rho_i^{a(k)}(r_{ij}) = \rho_{i0} \exp \left[-\beta_i^{(k)} \left(\frac{r_{ij}}{r_i^0} - 1 \right) \right], \quad (\text{A10})$$

where r_i^0 is the nearest-neighbor distance in the single-element reference structure and $\beta_i^{(k)}$ is element-dependent parameter. Finally, the average weighting factors are given by

$$t_i^{(k)} = \frac{\sum_{j \neq i} t_{0,j}^{(k)} \rho_j^{a(0)} S_{ij}}{\sum_{j \neq i} (t_{0,j}^{(k)})^2 \rho_j^{a(0)} S_{ij}}, \quad (\text{A11})$$

where $t_{0,j}^{(k)}$ is an element-dependent parameter.

The pair potential is given by

$$\phi_{ij}(r_{ij}) = \bar{\phi}_{ij}(r_{ij}) S_{ij}, \quad (\text{A12})$$

$$\bar{\phi}_{ij}(r_{ij}) = \frac{1}{Z_{ij}} \left\{ 2E_{ij}^u(r_{ij}) - F_i \left[\frac{Z_{ij}}{Z_i} \rho_j^{a(0)}(r_{ij}) \right] - F_j \left[\frac{Z_{ij}}{Z_j} \rho_j^{a(0)}(r_{ij}) \right] \right\}, \quad (\text{A13})$$

$$E_{ij}^u(r_{ij}) = -E_{ij}[1 + a_{ij}^*(r_{ij})] e^{-a_{ij}^*(r_{ij})}, \quad (\text{A14})$$

$$a_{ij}^* = \alpha_{ij} \left(\frac{r_{ij}}{r_{ij}^0} - 1 \right), \quad (\text{A15})$$

where E_{ij} , α_{ij} and r_{ij}^0 are element-dependent parameters and Z_{ij} depends upon the structure of the reference system. The background densities $\hat{\rho}_i(r_{ij})$ in Eq. (A13) are the densities for the reference structure computed with interatomic spacing r_{ij} .

The screening function S_{ij} is designed so that $S_{ij} = 1$ if atoms i and j are unscreened and within the cutoff radius r_c , and $S_{ij} = 0$ if they are completely screened or outside the cutoff radius. It varies smoothly between 0 and 1 for partial screening. The total screening function is the product of a

radial cutoff function and three body terms involving all other atoms in the system:

$$S_{ij} = \bar{S}_{ij} f_c \left(\frac{r_c - r_{ij}}{\Delta r} \right), \quad (\text{A16a})$$

$$\bar{S}_{ij} = \prod_{k \neq i, j} S_{ikj}, \quad (\text{A16b})$$

$$S_{ikj} = f_c \left(\frac{C_{ikj} - C_{\min,ijk}}{C_{\max,ijk} - C_{\min,ijk}} \right), \quad (\text{A16c})$$

$$C_{ikj} = 1 + 2 \frac{r_{ij}^2 r_{ik}^2 + r_{ij}^2 r_{jk}^2 - r_{ij}^4}{r_{ij}^4 - (r_{ik}^2 - r_{jk}^2)^2}, \quad (\text{A16d})$$

$$f_c(x) = \begin{cases} 1, & x \geq 1, \\ [1 - (1 - x)^4]^2, & 0 < x < 1, \\ 0, & x \leq 0. \end{cases} \quad (\text{A16e})$$

Note that C_{\min} and C_{\max} can be defined separately for each $i-j-k$ triplet, based on their element types. The parameter Δr controls the distance over which the radial cutoff is smoothed from 1 to 0 near $r = r_c$.

APPENDIX B: EQUILIBRIUM LATTICE PARAMETER AND BULK MODULUS

MEAM postulates the Rose universal equation of state¹⁴⁹

$$E_R(a^*) = -E_c \left(1 + a^* + \delta \frac{\alpha a^{*3}}{\alpha + a^*} \right) e^{-a^*} \quad (\text{B1})$$

for the reference structure of each single element and for each element pair. The a^* , scaled distance from the equilibrium nearest neighbor position r_0 , is

$$a^* = \alpha(r/r_0 - 1). \quad (\text{B2})$$

Two δ parameters may be specified for each element/pair: δ_r for negative and δ_a for positive a^* . Then

$$\delta = \begin{cases} \delta_r & \text{for } a^* < 0, \\ \delta_a & \text{for } a^* \geq 0. \end{cases} \quad (\text{B3})$$

^{*}Presently at Institute of Mechanics and Fluid Dynamics, TU Bergakademie Freiberg, Lampadiusstr. 4, 09596 Freiberg, Germany.

[†]Also at Department of Mechanical Engineering, Mississippi State University, Mississippi State, MS 39762, USA.

[‡]Also at Center for Computational Sciences, Mississippi State University, Mississippi State, MS 39762, USA.

[§]Also at Los Alamos National Laboratory, MST-8, MS G755, Los Alamos, NM 87545, USA.

¹M. F. Horstemeyer, in *Practical Aspects Computational Chemistry*, edited by J. Leszczynski and M. K. Shukla (Springer, Netherlands, 2010), pp. 87–135.

²M. S. Daw and M. I. Baskes, *Phys. Rev. Lett.* **50**, 1285 (1983).

³M. S. Daw and M. I. Baskes, *Phys. Rev. B* **29**, 6443 (1984).

⁴M. I. Baskes, *Phys. Rev. Lett.* **59**, 2666 (1987).

⁵M. S. Daw, *Phys. Rev. B* **39**, 7441 (1989).

⁶M. I. Baskes, J. S. Nelson, and A. F. Wright, *Phys. Rev. B* **40**, 6085 (1989).

The MEAM potential parameter α is related to the equilibrium atomic volume Ω_0 , the bulk modulus B_0 , and the cohesive energy of the reference structure E_c as follows:

$$\alpha = \sqrt{\frac{9B_0\Omega_0}{E_c}}. \quad (\text{B4})$$

The DFT equilibrium energies and bulk moduli were obtained by fitting the energy-volume dependence to Murnaghan equation of state,¹⁵⁰

$$E(V) = E(V_0) + \frac{B_0 V}{B'_0(B'_0 - 1)} \times \left[B'_0 \left(1 - \frac{V_0}{V} \right) + \left(\frac{V_0}{V} \right)^{B'_0} - 1 \right]. \quad (\text{B5})$$

APPENDIX C: TRIGONAL AND TETRAGONAL SHEAR MODULUS

For small deformations of a cubic crystal, the change of energy density due to straining is

$$\Delta E_V = \frac{1}{2} C_{11} (\epsilon_1^2 + \epsilon_2^2 + \epsilon_3^2) + C_{12} (\epsilon_1 \epsilon_2 + \epsilon_2 \epsilon_3 + \epsilon_3 \epsilon_1) + \frac{1}{2} C_{44} (\epsilon_4^2 + \epsilon_5^2 + \epsilon_6^2) + O(\epsilon_i^3), \quad (\text{C1})$$

where ϵ_i are strains in modified Voigt notation.

The trigonal shear modulus C_{44} was determined from rhombohedral deformation given by $\epsilon_1 = \epsilon_2 = \epsilon_3 = 0$ and $\epsilon_4 = \epsilon_5 = \epsilon_6 = \delta$ in Eq. (C1), leading to

$$\Delta E_V(\delta) = \frac{3}{2} C_{44} \delta^2 + O(\delta^3). \quad (\text{C2})$$

The tetragonal shear modulus $(C_{11} - C_{12})/2$ was determined from the deformation given by $\epsilon_1 = \delta, \epsilon_2 = \frac{1}{1+\delta} - 1$ in Eq. (C1), leading to

$$\Delta E_V(\delta) = (C_{11} - C_{12}) \delta^2 + O(\delta^3). \quad (\text{C3})$$

The (C2) and (C3) were used to estimate tetragonal and trigonal shear moduli.

⁷M. I. Baskes, *Phys. Rev. B* **46**, 2727 (1992).

⁸M. I. Baskes, J. E. Angelo, and C. L. Bisson, *Modell. Simul. Mater. Sci. Eng.* **2**, 505 (1994).

⁹K. Gall, M. F. Horstemeyer, M. van Schilfgaarde, and M. I. Baskes, *J. Mech. Phys. Solids.* **48**, 2183 (2000).

¹⁰B.-J. Lee and M. I. Baskes, *Phys. Rev. B* **62**, 8564 (2000).

¹¹H. Huang, N. M. Ghoniem, J. K. Wong, and M. I. Baskes, *Modell. Simul. Mater. Sci. Eng.* **3**, 615 (1995).

¹²M. I. Baskes, *Mater. Chem. Phys.* **50**, 152 (1997).

¹³M. I. Baskes, *Mater. Sci. Eng. A* **261**, 165 (1999).

¹⁴B.-J. Lee, J.-H. Shim, and M. I. Baskes, *Phys. Rev. B* **68**, 144112 (2003).

¹⁵W. Hu, B. Zhang, B. Huang, F. Gao, and D. J. Bacon, *J. Phys.: Condens. Matter* **13**, 1193 (2001).

¹⁶W. Hu, H. Deng, X. Yuan, and M. Fukumoto, *Eur. Phys. J. B* **34**, 429 (2003).

¹⁷B.-J. Lee and J. W. Lee, *Calphad* **29**, 7 (2005).

- ¹⁸B.-J. Lee, W.-S. Ko, H.-K. Kim, and E.-H. Kim, *Calphad* **34**, 510 (2010).
- ¹⁹K. Kang and W. Cai, *Philos. Mag.* **87**, 2169 (2007).
- ²⁰T. S. Gates, G. M. Odegard, S. J. V. Frankland, and T. C. Clancy, *Compos. Sci. Technol.* **65**, 2416 (2005).
- ²¹S. J. Noronha and D. Farkas, *Phys. Rev. B* **66**, 132103 (2002).
- ²²E. Martínez, J. Marian, A. Arsenil, M. Victoria, and J. Perlado, *J. Mech. Phys. Solids* **56**, 869 (2008).
- ²³G. P. Potirniche, M. F. Horstemeyer, G. J. Wagner, and P. M. Gullett, *Int. J. Plast.* **22**, 257 (2006).
- ²⁴H. van Swygenhoven, P. M. Derlet, and A. G. Frøseth, *Nat. Mater.* **3**, 399 (2004).
- ²⁵R. A. Johnson and D. J. Oh, *J. Mater. Res.* **4**, 1195 (1989).
- ²⁶R. A. Johnson, *Phys. Rev. B* **39**, 12554 (1989).
- ²⁷X. W. Zhou, H. N. G. Wadley, R. A. Johnson, D. J. Larson, N. Tabat, A. Cerezo, A. K. Petford-Long, G. D. W. Smith, P. H. Clifton, R. L. Martens, and T. F. Kelly, *Acta Mater.* **49**, 4005 (2001).
- ²⁸X. W. Zhou, R. A. Johnson, and H. N. G. Wadley, *Phys. Rev. B* **69**, 144113 (2004).
- ²⁹Y. Mishin, M. J. Mehl, and D. A. Papaconstantopoulos, *Acta Mater.* **53**, 4029 (2005).
- ³⁰M. I. Mendelev, M. Asta, M. J. Rahman, and J. J. Hoyt, *Philos. Mag.* **89**, 3269 (2009).
- ³¹X. Y. Liu and J. B. Adams, *Acta Mater.* **46**, 3467 (1998).
- ³²F. Apostol and Y. Mishin, *Phys. Rev. B* **83**, 054116 (2011).
- ³³X.-Y. Liu, C.-L. Liu, and L. J. Borucki, *Acta Mater.* **47**, 3227 (1999).
- ³⁴M. I. Mendelev, D. J. Srolovitz, G. J. Ackland, and S. Han, *J. Mater. Res.* **20**, 208 (2005).
- ³⁵T. Ohira, Y. Inoue, K. Murata, and J. Murayama, *Appl. Surf. Sci.* **171**, 175 (2001); T. Ohira and Y. Inoue, *MRS Proceedings* **492**, 401 (1997).
- ³⁶S. M. Valone, M. I. Baskes, and R. L. Martin, *Phys. Rev. B* **73**, 214209 (2006).
- ³⁷H.-K. Kim, W.-S. Jung, and B.-J. Lee, *Acta Mater.* **57**, 3140 (2009).
- ³⁸K.-H. Kang, I. Sa, J.-C. Lee, E. Fleury, and B.-J. Lee, *Scr. Mater.* **61**, 801 (2009).
- ³⁹E. C. Do, Y.-H. Shin, and B.-J. Lee, *J. Phys.: Condens. Matter* **21**, 325801 (2009).
- ⁴⁰H.-K. Kim, W.-S. Jung, and B.-J. Lee, *J. Mater. Res.* **25**, 1288 (2010).
- ⁴¹K. Chenoweth, A. C. T. van Duin, and W. A. Goddard, *J. Phys. Chem. A* **112**, 1040 (2008).
- ⁴²J. E. Angelo, N. R. Moody, and M. I. Baskes, *Modell. Simul. Mater. Sci. Eng.* **3**, 289 (1995); M. I. Baskes, X. Sha, J. E. Angelo, and N. R. Moody, *ibid.* **5**, 651 (1997).
- ⁴³Y. Q. Cheng, E. Ma, and H. W. Sheng, *Phys. Rev. Lett.* **102**, 245501 (2009).
- ⁴⁴G. Bonny, R. C. Pasianot, N. Castin, and L. Malerba, *Philos. Mag.* **89**, 3531 (2009).
- ⁴⁵B. Jelinek, ASE Atomistic Potential Tests, [<http://code.google.com/p/ase-atomistic-potential-tests>] (2011).
- ⁴⁶P. E. Blöchl, *Phys. Rev. B* **50**, 17953 (1994); G. Kresse and D. Joubert, *ibid.* **59**, 1758 (1999).
- ⁴⁷G. Kresse and J. Hafner, *Phys. Rev. B* **47**, 558 (1993); G. Kresse and J. Furthmüller, *ibid.* **54**, 11169 (1996).
- ⁴⁸J. P. Perdew, J. A. Chevary, S. H. Vosko, K. A. Jackson, M. R. Pederson, D. J. Singh, and C. Fiolhais, *Phys. Rev. B* **46**, 6671 (1992).
- ⁴⁹H. J. Monkhorst and J. D. Pack, *Phys. Rev. B* **13**, 5188 (1976).
- ⁵⁰B. Jelinek, J. Houze, S. Kim, M. F. Horstemeyer, M. I. Baskes, and S.-G. Kim, *Phys. Rev. B* **75**, 054106 (2007).
- ⁵¹T. Lee, M. I. Baskes, S. M. Valone, and J. D. Doll, *J. Phys.: Condens. Matter* **24**, 225404 (2012).
- ⁵²X.-Y. Liu, P. Ohotnický, J. Adams, C. Rohrer, and R. Hyland, *Surf. Sci.* **373**, 357 (1997).
- ⁵³A. F. Wright, *Phys. Rev. B* **74**, 165116 (2006).
- ⁵⁴P. Tzanetakis, J. Hillairet, and G. Revel, *Phys. Status Solidi B* **75**, 433 (1976).
- ⁵⁵K. M. Carling, G. Wahnström, T. R. Mattsson, N. Sandberg, and G. Grimvall, *Phys. Rev. B* **67**, 054101 (2003).
- ⁵⁶T. Hehenkamp, *J. Phys. Chem. Solids* **55**, 907 (1994).
- ⁵⁷D. A. Andersson and S. I. Simak, *Phys. Rev. B* **70**, 115108 (2004).
- ⁵⁸S. Dannefaer, P. Mascher, and D. Kerr, *Phys. Rev. Lett.* **56**, 2195 (1986); J. Throwe, T. C. Leung, B. Nielsen, H. Huomo, and K. G. Lynn, *Phys. Rev. B* **40**, 12037 (1989).
- ⁵⁹T. Hehenkamp, W. Berger, J.-E. Kluit, C. Lüdecke, and J. Wolff, *Phys. Rev. B* **45**, 1998 (1992).
- ⁶⁰H. Krimmel and M. Fähnle, *Phys. Rev. B* **62**, 5489 (2000).
- ⁶¹M. I. Mendelev, D. J. Srolovitz, G. J. Ackland, D. Y. Sun, and M. Asta, *Philos. Mag.* **83**, 3977 (2003).
- ⁶²G. J. Ackland, D. J. Bacon, A. F. Calder, and T. Harry, *Philos. Mag. A* **75**, 713 (1997).
- ⁶³C. Domain and C. S. Becquart, *Phys. Rev. B* **65**, 024103 (2001).
- ⁶⁴H.-E. Schaefer, K. Maire, M. Weller, D. Herlach, A. Seeger, and J. Diehl, *Scr. Metall.* **11**, 803 (1977).
- ⁶⁵M. I. Mendelev, M. J. Kramer, C. A. Becker, and M. Asta, *Philos. Mag.* **88**, 1723 (2008).
- ⁶⁶Y. Mishin, M. J. Mehl, D. A. Papaconstantopoulos, A. F. Voter, and J. D. Kress, *Phys. Rev. B* **63**, 224106 (2001).
- ⁶⁷M. Timonova, B.-J. Lee, and B. J. Thijssse, *Nucl. Instrum. Methods Phys. Res., Sect. B* **255**, 195 (2007).
- ⁶⁸S. Ryu, C. R. Weinberger, M. I. Baskes, and W. Cai, *Modell. Simul. Mater. Sci. Eng.* **17**, 075008 (2009).
- ⁶⁹S. Ramos de Debiaggi, M. de Koning, and A. M. Monti, *Phys. Rev. B* **73**, 104103 (2006).
- ⁷⁰G. P. Purja Pun and Y. Mishin, *Acta Mater.* **57**, 5531 (2009).
- ⁷¹N. Sandberg, B. Magyari-Köpe, and T. R. Mattsson, *Phys. Rev. Lett.* **89**, 065901 (2002).
- ⁷²B. A. Gillespie, X. W. Zhou, D. A. Murdick, H. N. G. Wadley, R. Drautz, and D. G. Pettifor, *Phys. Rev. B* **75**, 155207 (2007).
- ⁷³J. Tersoff, *Phys. Rev. B* **38**, 9902 (1988).
- ⁷⁴P. Erhart and K. Albe, *Phys. Rev. B* **71**, 035211 (2005).
- ⁷⁵O. K. Al-Mushadani and R. J. Needs, *Phys. Rev. B* **68**, 235205 (2003).
- ⁷⁶S.-G. Kim, M. F. Horstemeyer, M. I. Baskes, M. Rais-Rohani, S. Kim, B. Jelinek, J. Houze, A. Moitra, and L. Liyanage, *J. Eng. Mater. Technol.* **131**, 041210 (2009).
- ⁷⁷M. I. Mendelev, S. Han, D. J. Srolovitz, G. J. Ackland, D. Y. Sun, and M. Asta, *Philos. Mag.* **83**, 3977 (2003).
- ⁷⁸S. L. Dudarev and P. M. Derlet, *J. Phys.: Condens. Matter* **17**, 7097 (2005).
- ⁷⁹C.-C. Fu, F. Willaime, and P. Ordejón, *Phys. Rev. Lett.* **92**, 175503 (2004).
- ⁸⁰B. J. Jesson, M. Foley, and P. A. Madden, *Phys. Rev. B* **55**, 4941 (1997).
- ⁸¹L. Vitos, A. V. Ruban, H. L. Skriver, and J. Kollár, *Surf. Sci.* **411**, 186 (1998).
- ⁸²F. De Boer, R. Boom, W. Mattens, A. Miedema, and A. Niessen, *Cohesion in Metals: Transition Metal Alloys*, edited by F. R.

- de Boer and D. G. Pettifor, Vol. 1 (North-Holland, Amsterdam, 1988).
- ⁸³J. H. Wilson, J. D. Todd, and A. P. Sutton, *J. Phys.: Condens. Matter* **2**, 10259 (1990).
- ⁸⁴M. Timonova and B. J. Thijssse, *Modell. Simul. Mater. Sci. Eng.* **19**, 015003 (2011).
- ⁸⁵A. A. Stekolnikov, J. Furthmüller, and F. Bechstedt, *Phys. Rev. B* **65**, 115318 (2002).
- ⁸⁶D. J. Eaglesham, A. E. White, L. C. Feldman, N. Moriya, and D. C. Jacobson, *Phys. Rev. Lett.* **70**, 1643 (1993).
- ⁸⁷X. Y. Liu, C. L. Liu, and L. J. Borucki, *Acta Mater.* **47**, 3227 (1999).
- ⁸⁸P. Błoński and A. Kiejna, *Surf. Sci.* **601**, 123 (2007).
- ⁸⁹H. Balamane, T. Halicioglu, and W. A. Tiller, *Phys. Rev. B* **46**, 2250 (1992).
- ⁹⁰A. E. Mattsson and W. Kohn, *J. Chem. Phys.* **115**, 3441 (2001).
- ⁹¹R. Armiento and A. E. Mattsson, *Phys. Rev. B* **72**, 085108 (2005).
- ⁹²J. P. Perdew, A. Ruzsinszky, G. I. Csonka, O. A. Vydrov, G. E. Scuseria, L. A. Constantin, X. Zhou, and K. Burke, *Phys. Rev. Lett.* **100**, 136406 (2008).
- ⁹³A. E. Mattsson, R. Armiento, P. A. Schultz, and T. R. Mattsson, *Phys. Rev. B* **73**, 195123 (2006).
- ⁹⁴R. Peierls, *Proc. Phys. Soc. London* **52**, 34 (1940).
- ⁹⁵F. R. N. Nabarro, *Proc. Phys. Soc. London* **59**, 256 (1947).
- ⁹⁶P. Carrez, D. Ferré, and P. Cordier, *Modell. Simul. Mater. Sci. Eng.* **17**, 035010 (2009).
- ⁹⁷V. Vítek, *Phys. Status Solidi* **18**, 687 (1966).
- ⁹⁸J. A. Zimmerman, H. Gao, and F. F. Abraham, *Modell. Simul. Mater. Sci. Eng.* **8**, 103 (2000).
- ⁹⁹A. Datta, U. V. Waghmare, and U. Ramamurty, *Acta Mater.* **56**, 2531 (2008).
- ¹⁰⁰M. Mihalkovic and M. Widom, *Alloy database* [<http://euler.phys.cmu.edu/alloy/>] (2009).
- ¹⁰¹C. Ravi, C. Wolverton, and V. Ozoliņš, *Europhys. Lett.* **73**, 719 (2006).
- ¹⁰²C. Wolverton and V. Ozoliņš, *Phys. Rev. Lett.* **86**, 5518 (2001).
- ¹⁰³J. L. Murray, *Int. Met. Rev.* **30**, 211 (1985).
- ¹⁰⁴C. Ravi and C. Wolverton, *Metall. Mater. Trans. A* **36**, 2013 (2005).
- ¹⁰⁵R. Besson and J. Morillo, *Phys. Rev. B* **55**, 193 (1997).
- ¹⁰⁶L. Shaojun, D. Suqing, and M. Benkun, *Phys. Rev. B* **58**, 9705 (1998).
- ¹⁰⁷W.-q. Zhang, Q. Xie, X.-j. Ge, and N.-x. Chen, *J. Appl. Phys.* **82**, 578 (1997).
- ¹⁰⁸S. Meschel and O. Kleppa, *Metall. Mater. Trans. A* **22**, 2162 (1991).
- ¹⁰⁹S. J. Solares, Ph.D. thesis, California Institute of Technology, 2006.
- ¹¹⁰E. G. Moroni, W. Wolf, J. Hafner, and R. Podloucky, *Phys. Rev. B* **59**, 12860 (1999).
- ¹¹¹S. Zhou, Y. Wang, F. Shi, F. Sommer, L.-Q. Chen, Z.-K. Liu, and R. Napolitano, *J. Phase Equilib. Diffus.* **28**, 158 (2007).
- ¹¹²S. Narasimhan and J. W. Davenport, *Phys. Rev. B* **51**, 659 (1995).
- ¹¹³Y. Zhong, M. Yang, and Z.-K. Liu, *Calphad* **29**, 303 (2005).
- ¹¹⁴N. Wang, W.-Y. Yu, B.-Y. Tang, L.-M. Peng, and W.-J. Ding, *J. Phys. D* **41**, 195408 (2008).
- ¹¹⁵Y.-M. Kim, N. J. Kim, and B.-J. Lee, *Calphad* **33**, 650 (2009).
- ¹¹⁶X.-Y. Liu, P. P. Ohotnický, J. B. Adams, C. L. Rohrer, and R. W. Hyland, *Surf. Sci.* **373**, 357 (1997).
- ¹¹⁷J. Murray, *J. Phase Equilib.* **3**, 60 (1982).
- ¹¹⁸P. Villars and L. D. Calvert, *Pearson's Handbook of Crystallographic Data for Intermetallic Phases* (American Society for Metals, Materials Park, OH, 1985).
- ¹¹⁹D. Singh, C. Suryanarayana, L. Mertus, and R.-H. Chen, *Intermetallics* **11**, 373 (2003).
- ¹²⁰S. G. Fries and T. Jantzen, *Thermochim. Acta* **314**, 23 (1998).
- ¹²¹X.-Y. Liu, Ph.D. thesis, University of Illinois at Urbana-Champaign, (1997).
- ¹²²P. Maugis, J. Lacaze, R. Besson, and J. Morillo, *Metall. Mater. Trans. A* **37**, 3397 (2006).
- ¹²³P. G. Gonzales-Ormeño, H. M. Petrilli, and C. G. Schön, *Calphad* **26**, 573 (2002).
- ¹²⁴R. E. Watson and M. Weinert, *Phys. Rev. B* **58**, 5981 (1998).
- ¹²⁵N. I. Kulikov, A. V. Postnikov, G. Borstel, and J. Braun, *Phys. Rev. B* **59**, 6824 (1999).
- ¹²⁶M. Friák and J. Neugebauer, *Intermetallics* **18**, 1316 (2010).
- ¹²⁷F. Lechermann, M. Fähnle, and J. M. Sanchez, *Intermetallics* **13**, 1096 (2005).
- ¹²⁸C. L. Fu and M. H. Yoo, *Acta Metall. Mater.* **40**, 703 (1992).
- ¹²⁹E. Lee and B.-J. Lee, *J. Phys.: Condens. Matter* **22**, 175702 (2010).
- ¹³⁰X. Shu, W. Hu, H. Xiao, H. Deng, and B. Zhang, *J. Mater. Sci. Technol. (Shenyang, China)* **17**, 601 (2001).
- ¹³¹C. Vailhé and D. Farkas, *Acta Mater.* **45**, 4463 (1997).
- ¹³²O. Kubaschewski and W. A. Dench, *Acta Metall.* **3**, 339 (1955).
- ¹³³P. D. Desai, *J. Phys. Chem. Ref. Data* **16**, 109 (1987).
- ¹³⁴R. Hultgren, P. D. Desai, D. T. Hawkins, M. Gleiser, and K. K. Kelley, *Selected Values of the Thermodynamic Properties of Binary Alloys* (American Society for Metals, Metals Park, OH, 1973).
- ¹³⁵*Smithells Metals Reference Book*, 7th ed., edited by E. A. Brandes and G. B. Brook (Butterworth-Heinemann, Oxford, 1992).
- ¹³⁶W. B. Pearson, *A Handbook of Lattice Spacings and Structures of Metals and Alloys* (Pergamon Press, New York, 1958).
- ¹³⁷M. H. Yoo, T. Takasugi, S. Hanada, and O. Izumi, *Mater. Trans., JIM* **31**, 435 (1990).
- ¹³⁸G. Simmons and H. Wang, *Single Crystal Elastic Constants and Calculated Aggregate Properties* (MIT Press, Cambridge, MA, 1971).
- ¹³⁹M. Krajčí and J. Hafner, *J. Phys.: Condens. Matter* **14**, 5755 (2002).
- ¹⁴⁰N. P. Bailey, J. Schiøtz, and K. W. Jacobsen, *Phys. Rev. B* **69**, 144205 (2004).
- ¹⁴¹R. C. King and O. J. Kleppa, *Acta Metall.* **12**, 87 (1964).
- ¹⁴²B. Predel and H. Ruge, *Mater. Sci. Eng.* **9**, 333 (1972).
- ¹⁴³*Metals Handbook Desk Edition*, 2nd ed., edited by J. R. Davis (ASM International, Materials Park, OH, 1998).
- ¹⁴⁴J. J. Chu and C. A. Steeves, *J. Non-Cryst. Solids* **357**, 3765 (2011).
- ¹⁴⁵A. J. C. Wilson, *Proc. Phys. Soc.* **53**, 235 (1941).
- ¹⁴⁶S. J. Plimpton, *J. Comput. Phys.* **117**, 1 (1995).
- ¹⁴⁷S. R. Bahn and K. W. Jacobsen, *Comput. Sci. Eng.* **4**, 56 (2002).
- ¹⁴⁸C. A. Becker, in *Models, Databases, and Simulation Tools Needed for the Realization of Integrated Computational Materials Engineering*, Proceedings of the Symposium Held at Materials Science and Technology 2010, Houston, Texas, USA, edited by S. M. Arnold and T. T. Wong (ASM International, Materials Park, OH, 2011); C. A. Becker, *Atomistic Simulations for Engineering: Potentials and Challenges* [<http://www.ctcms.nist.gov/potentials>].
- ¹⁴⁹J. H. Rose, J. R. Smith, F. Guinea, and J. Ferrante, *Phys. Rev. B* **29**, 2963 (1984).
- ¹⁵⁰F. D. Murnaghan, *Proc. Natl. Acad. Sci. USA* **30**, 244 (1944).